Analysis of composites using peridynamics

Corrado Degl'Incerti Tocci

Thesis submitted to the Faculty of the

Virginia Polytechnic Institute and State University

in partial fulfillment of the requirements for the degree of

Master of Science

in

Aerospace Engineering

Gary D. Seidel, Chair

Mayuresh J. Patil

Michael K. Philen

December 10, 2013

Blacksburg, Virginia

Keywords: peridynamics, multiscale, carbon nanotube, finite element analysis, truss, micromechanics

Analysis of composites using peridynamics

Corrado Degl'Incerti Tocci

(ABSTRACT)

Since the last century a lot of effort has been spent trying to analyze damage and crack evolution in solids. This field is of interest because of the many applications that require the study of the behavior of materials at the micro- or nanoscale, i.e. modeling of composites and advanced aerospace applications. Peridynamics is a recently developed theory that substitutes the differential equations that constitute classical continuum mechanics with integral equations. Since integral equations are valid at discontinuities and cracks, peridynamics is able to model fracture and damage in a more natural way, without having to work around mathematical singularities present in the classical continuum mechanics theory. The objective of the present work is to show how peridynamics can be implemented in finite element analysis (FEA) using a mesh of one-dimensional truss elements instead of 2-D surface elements. The truss elements can be taken as a representation of the bonds between molecules or particles in the body and their strength is found according to the physical properties of the material. The possibility implementing peridynamics in a finite element framework, the most used method for structural analysis, is critical for expanding the range of problems that can be analyzed, simplifying the verification of the code and for making fracture analysis computationally cheaper. The creation of an in-house code allows for easier modifications, customization and enrichment if more complex cases (such as multiscale modeling of composites or piezoresistive materials) are to be analyzed. The problems discussed in the present thesis involve plates with holes and inclusions subjected to tension. Displacement boundary conditions are applied in all cases. The results show good agreement with theory as well as with empirical observation. Stress concentrations reflect the behavior of materials in real life, cracks spontaneously initiate and debonding naturally happens at the right locations. Several examples clearly show this behavior and prove that peridynamics is a promising tool for stress and fracture analysis.

Acknowledgments

First, I would like to thank my advisor, Dr. Gary Seidel, without whom all this would not have been possible. His support and encouragement were unvaluable, as well as his professional guidance. His passion for learning and teaching sets a standard hardly reachable by anyone and his humility and empathy make him a great all-around person. Dr. Seidel's trust in me is what kept me going, allowing me to complete this chapter of my life.

I would like to thank Adarsh Chaurasia, Skylar Stevens, Xiang Ren and Yumeng Li for their help in finding the cohesive zone solutions and preparing some extra meshes for me, which gave me more ways to check my results, increasing the value of this work. I would also like to thank Naveen Prakash, whose help and constructive critics were fundamental in gaining a deeper understanding of the subject.

I would like to thank my parents Fabrizio and Lelia who always supported me, especially in the most difficult moments, even from so far away. You always motivated me to reach for higher goals and go my own way, even if that took me away from you. A special thanks goes to my sister Letizia, who I have always looked up to; she is one of the best people I know and I feel incredibly lucky to have her as a sister.

I would like to thank the coach of the varsity tennis team, Jim Thompson, who always helped me when I was in trouble and when I was overwhelmed with work. Jim was much more than a coach to me: he was a tutor, a counselor, an advisor and a friend; without him I probably would not have made it through college.

A final thought goes to all the friends I made in these five great years at Virginia Tech. All of you were fundamental to my small success, meeting you opened my mind in hundreds of different ways and helped me grow as a person. To my friends in Italy, thanks for bearing with me when I was gone and for being patient when I was back home. Long-lasting friendships are difficult to achieve and I am incredibly fortunate to still have you in my life after so many years. A special thanks goes to my girlfriend, Letizia, who was kind enough to stay with me for more than five years from thousands of miles away. Thank you for understanding my decision to go and not holding it against me (all the time). I would not have made it without you.

Contents

List of Figures

Chapter 1

Introduction

The last two decades have seen a dramatic improvement in computational power, which led to much higher accuracy in computer simulations. The fields of mechanics and material science have become increasingly interested in exploiting this power by building simulations that have the duty to anticipate and predict the behavior of different materials under various types of loading and boundary conditions [7]. Accurate simulations require very specific tools, both computational and experimental, as well as a deep understanding of the chemistry and physics at the atomic, molecular and supramolecular levels [1].

The design of objects and vehicles with a very low factor of safety is another push towards increasing accuracy of computer simulations; the challenges in modeling of these vehicles are related to the improvement of the performance of aircrafts and spacecraft by increasing: size per mass, strength per mass, function per mass and power, and intelligence per mass and power [1]. To achieve these goals, composite materials are used more extensively in space and high-technology applications, because they can be designed and manufactured to have specific characteristics and to meet specific requirements [1]. Because the mechanical and electrical properties of composite materials tend to be very difficult to obtain [8], computational methods are being researched to study the behavior of these materials at smaller length scales, which can be the key to a

deeper understanding of the interaction between the different phases. A particular case is represented by nanocomposites, which have shown to behave often in unpredictable ways. Different methods are employed to find their effective mechanical and electrical properties [9] and there is a lot of research focused on how to predict the behavior of carbon nanotubes, or carbon fiber, composites. Because of the increasing computational power of today's computers, the modeling problem is dealt with using computational methods paired with testing and direct observation [7]. Still, computational power is not yet great enough to model every single atom or molecule for macroscopic systems [5]. The problem that this lack of power poses can be reduced by techniques that force us to make assumptions and reduce the accuracy of the model, but making it realizable on the other hand. One of these techniques is called multiscale modeling: it means analyzing a given problem at different lengh scales, using different methods which are consistent with each other, as shown in Figure 1.1. This approach is fundamental in micromechanics and allows us to reduce computational power in many applications, because we do not need as much accuracy in analyzing phenomena with negligible microscale effects. Nonetheless, multiscale modeling poses some questions with no easy answer: how is the information passed from one layer to the next? How do we precisely circumscribe the area of interest (or size of interest)? What is lost in accuracy when applying less expensive methods at greater length scales? These are all questions that need to be asked in order to understand the importance of a well-posed problem.

The goal of this work is to validate and study the applications of a nonlocal continuum theory called Peridynamics (PD), proposed by Silling from Sandia National Laboratories in 2000 [10]. The validation is performed by implementing peridynamics in a finite elements framework, which is supposed to reduce computational power and simplify the model, making is suitable to a wider range of applications. An implementation of peridynamics can be found in [11], where three problems are solved implementing peridynamics in ABAQUS; this approach, although easier and more direct, is more subject to restrictions and allows for a limited range of applications. The aim of the present work is to create a coding platform in Matlab, which is highly customizable and can be later modified and enhanced to be applied in a greater range of problems like multiscale modeling of composites and piezoresistive materials. All the plots in this paper are done in TecPlot, which is

the only other piece of software used. Finally, the last objective of the present work is to apply peridynamics to the analysis of composite materials made of one or multiple fiber inclusions; this is not been done yet and this work can be seen as an introduction, a preliminary study of this kind of applications.

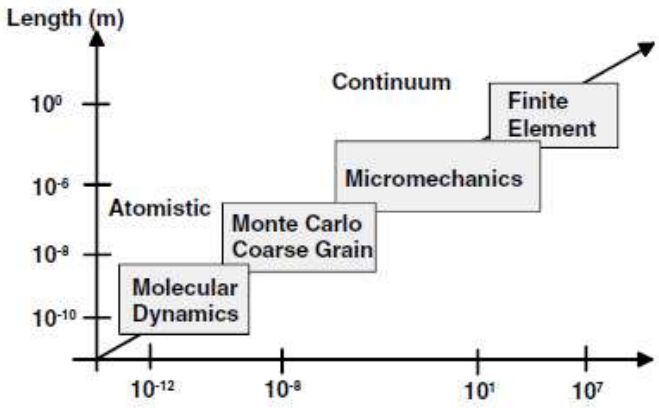

Figure 1.1: Hierarchy of multiscale modeling (from Ref [1]: Gates and Odegard and Frankland and Clancy, "Computational materials: Multi-scale modeling and simulation of nanostructured materials", *Composites Science and Technology*, 2005. Used with permission of Elsevier).

1.1 Brief History of Nonlocal Theories

The problem of crack propagation in solids has been studied for decades now. Because of its gradient formulation classical mechanics is not defined at discontinuities such as cracks [10]. At very small scales bodies do not behave as continua, but as a conglomerate of particles or atoms, hence a more 'atomistic' description of the material is needed. Cracks happen because of a rupture at the micro- or nanoscale and cannot be completely understood and studied within the boundaries of a continuum formulation, which does not take into consideration the microstructure of the material. Also, classical continuum mechanics is unable to find the stress concentration at the cracktip because of a mathematical singularity; high strain gradients near the crack make it impossible to have accurate results at this location and these factors make

propagation impossible to model in a classical continuum mechanics framework. In the last century scientists have started to take care of this lack of information by adding details to the classical theory of continuum mechanics [12]. These formulations are called nonlocal theories and it will be shown how the peridynamics theory belongs to this category. Three main families of nonlocal theories have been proposed through history to differentiate the way information is added to the classical model: *augmentation of the displacement field* (ADF), *augmentation of the gradient of the displacement field* (AGDF) and the use of an *integral operator* (IO) [13]. As it will be shown later, the difference between these families lies mostly in the type of nonlocality they employ.

The first effective formulation of the ADF kind was proposed by Cosserat and Cosserat in 1909 [14]. In their formulation the infinitesimal particle is enriched with three rotational degrees of freedom, hence improving the classical theory by adding complexity to it. In this formulation, the continuum mechanics solution becomes a special case of the Cosserats' theory. Their originally nonlinear development was largely forgotten for decades only to be rediscovered in a restricted linearized setting in the early sixties [15], first with Mindlin [16], then especially with Kunin [17], Kröner [18] and Edelen [19]. All these generalized Cosserat theories characterize the motion of a solid body by adding more fields that are independent of the displacement field and provide supplementary information on the small-scale kinematics [12]. The biggest contribution in the field arrives from Eringen [20, 21, 22, 23, 13] who also tried to unify and categorize these theories under the name of *micropolar*, where degrees of freedom are added and the particles behave as rigid bodies with rotational displacements as well. Eringen will also later define the terms *microstretch* and *micromorphic*: the former adds a "breathing mode" to the Cosserats rotations, a deformation in one direction only through which the infinitesimal body can expand and contract [24, 25]; the latter adds the remaining deformations in the other directions, bringing the total count of degrees of freedom to nine (three translations from the classical model, three Cosserats rotations, three deformations) [26]. It becomes obvious at this point that the micropolar and the microstretch cases are special cases of the most general micromorphic theory, respectively with zero deformation and with one non-zero deformation. Worth of a note is also Eringen's work in redefinfing

the concepts of locality and nonlocality; the meaning of these terms in the field of micromechanics will be explained in Section 1.2 and will be mostly based on Eringen's work [27, 28, 29].

The second family of generalized continua employs AGDF and comprises those formulations in which the displacement field is the only independent kinematic field (no enrichment in degrees of freedom of the infinitesimal element), while the resolution is improved by incorporating the gradients of strain (second gradients of displacement) into the constitutive equations [12]. Contributions in this field were given by Aero and Kuvshinskii [30], Grioli [31] and Rajagopal [32]. The work of these scientists consisted mostly in taking into account the curvature components of the strain gradient, i.e. the gradients of rotations. Decomposing the macroscopic deformation gradient allows us to obtain a rotation tensor for each material particle; hence, this theory is equivalent to Cosserat's, in which the rotations associated with each material particle are not independent [12]. Later, other extensions of the gradient theory were formulated. These include the effects of the stretch gradients (Toupin [33]), second strain gradients (Mindlin [34]) and gradients of all orders (Green and Rivlin [35]). Krumhansl [36] discussed the need for higher-order displacement gradients when approximating discrete lattices in a continuum mechanics framework [12]. As it can be easily shown, ADF and AGDF theories still do not offer a complete solution for the dynamic fracture case, since discontinuities cannot be throughly analyzed using a gradient (or differential) formulation.

The last family of generalized continua is the one of most interest for the present paper, since peridynamcs belongs to this category. It is represented by those micromechanics theories that implement an integral operator (IO) to perform weighted averaging over a spatial neighborhood to replace a certain variable by its nonlocal counterpart [37]. If $f(x)$ is some 'local' field in a domain V, the corresponding nonlocal field is defined by

$$\bar{f}(\mathbf{x}) = \int_V \alpha'(\mathbf{x}, \boldsymbol{\xi}) f(\boldsymbol{\xi}) \, \mathrm{d}\boldsymbol{\xi}, \tag{1.1.1}$$

where $\alpha'(\mathbf{x}, \boldsymbol{\xi})$ is a given nonlocal weight function [37].

The family of theories that can be written in the form of Eqn 1.1.1 are all strongly nonlocal (a discussion on nonlocality is given in Section 1.2). Nonlocal elasticity was analyzed and refined in many of the papers

mentioned in the last two paragraphs, namely Eringen [13], Eringen and Edelen [38] and Kröner [18]. Additional work includes Rogula [39] (who first proposed a nonlocal form of the constitutive law for elastic materials), Kröner [40, 41], Kröner and Datta [42], Kunin [43, 44], Edelen and Laws [45]. These early studies had the goal to create a better theory that would describe phenomena taking place on an atomic or molecular scale. It was shown that nonlocality adds information to the continuum model approximating the dispersion of short elastic waves, hence improving the description of the interactions inside and between crystals [12]. Since the 80s Bazant has been contributing to this field [46, 47], clarified some incongruences in the distinction between the generalized continua [12] and performed studies on nonlocal finite elements codes [48], which are a fundamental basis for the work presented in this thesis. In the last two decades Polizzotto expanded and gave additional bases to the strongly nonlocal theory with [49] and [50], in which he proposes a unified theory for the nonlocal/gradient continuum theories and establishes the framework in which this will take place. In chapter 2 it will be shown how peridynamics belongs to this last family of generalized continua and how its formulation differs from the ones analyzed so far; in fact, while in the integral formulations analyzed so far generally the strains are averaged over a certain domain, in peridynamics the force between each pair of particle is averaged, leading to a theory free of derivatives of displacement.

During the last 50 years it has become increasingly clear that distributed damage cannot be adequately described by local constitutive relations. So far only the analytical approach was described, which is limited by complicated geometries. For this reason computational models have been developed to fix this lack of potential applications. Classical finite element methods generally need remeshing, since cracks are discontinuities and no mesh can be applied inside such areas. Evolutions of the finite element method for fracture mechanics applications, such as XFEM or the Cohesive Zone Method, still employ differential equations in their formulation. Furthermore, additional information is generally needed to be able to model fracture, i.e. fracture initiation parameters, crack nucleation criteria, traction-displacement laws. Meshless methods have been developed as well, but incur in the same issues because they too are based on a differential formulation. Particle-based methods like Molecular Dynamics need to model individual atoms and molecules and are just

not applicable to macroscale problems because of the computational power needed.

1.2 Nonlocality

The concept of nonlocality marks the separation from the idea of continuum defined in classical continuum mechanics, for the state of the material at one point depends on the state of that material at the points not only in the immediate vicinity, but also at a certain distance from the point itself. Figure 1.2 graphically shows the difference between the local and nonlocal models: in (a) the exterior of the cube imparts force to the interior via the surface only, while in (b) the exterior of the cube imparts force to the interior not just at the surface, but also at a finite distance from the surface. A gradient-type nonlocal model, like AGDF

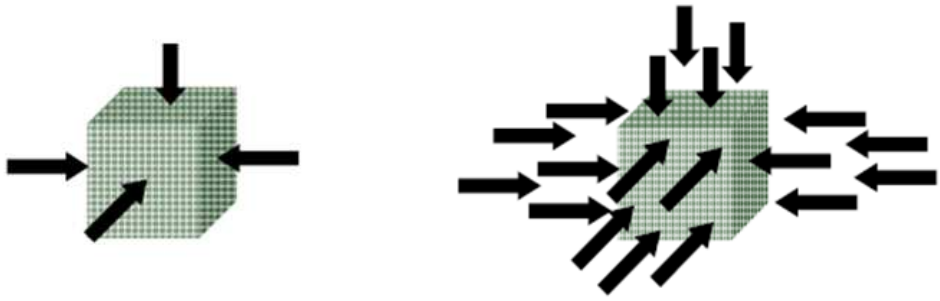

(a) Local model (b) Nonlocal model

Figure 1.2: Graphical representation of local and nonlocal models (from Ref [2]: Lehoucq, "Peridynamics for multiscale materials modeling", Sandia National Labs, Power Point Presentation, 2008. Used with permission of R. Lehoucq).

described in Section 1.1, adheres to this principle mathematically, by enriching the local constitutive relations with higher order gradients of some state variables. Gradient-types model exploit the concept of nonlocality in a broad sense, meaning that they employ a length scale, the meaning of which is explained in the next paragraph. To the narrow definition of nonlocal theories belongs the integral type model (IO), where the constitutive laws at a point involve weighted averages of a state variable over a certain neighborhood, which

can be discretionary large. Hence, strictly nonlocal theories are the ones described by integrodifferential equations, while strictly local theories are described by differential equations [12]. A mathematical definition of nonlocality has been formulated by Rogula in [51] and is given here. The fundamental equations of any physical theory can be written as

$$Au = f, \tag{1.2.1}$$

where A is the operator characterizing the system, u is the unknown response and f is the given excitation. Typically, u and f are functions or distributions defined over a certain spatial domain V. Operator A is called *local* if it has the following property: *if two functions u and v are identical in an open set O, then their images Au and Av are also identical in O*, which means that whenever $u(\mathbf{x}) = v(\mathbf{x})$ for all $\mathbf{x}$ in a neighborhood of point $\mathbf{x}_0$, then $Au(\mathbf{x}_0) = Av(\mathbf{x}_0)$. Since derivatives do not change if the differentiated function changes only outside a small neighborhood of the point at which derivatives are taken, we can see that differential operators satisfy this condition. If, on the other hand, we add an integral operator to consider the weighted average of a state variable, we obtain the following equation [51]:

$$\int_{-\infty}^{\infty} A(x)u(x)\,\mathrm{d}x = f(x); \tag{1.2.2}$$

due to the presence of the spatial integral, the locality condition is violated.

Another important aspect regarding the definition of nonlocality is the presence of a length scale. From the mathematical point of view, the presence of a length scale shows that the scaling of spatial coordinates has an effect on the fundamental equations [51]. Hence, in local theories, where a length scale is not present, the fundamental relations are invariant with respect to scaling of the spatial coordinates. Theories invariant with respect to spatial scaling are called *strictly local*, while theories not invariant with respect to spatial scaling are called *weakly non local*. Weakly nonlocal theories are usually described by differential equations, where the coefficients multiplying the terms of different orders have different physical dimensions which make it possible to deduce a length scale from the ratio [12]. In [5] this concept is explained clearly: consider the classical wave equation

$$\frac{\partial^2 y}{\partial t^2} = a\frac{\partial^2 y}{\partial x^2}, \tag{1.2.3}$$

which does not possess a length scale. Its solution is defined as *scale-invariant* by Barenblatt in [52]. Now consider the higher-order wave equation [5]

$$\frac{\partial^2 y}{\partial t^2} = a\frac{\partial^2 y}{\partial x^2} - b\frac{\partial^4 y}{\partial x^4} \tag{1.2.4}$$

where a and b are constant coefficients. Dimensional consistency of the terms in Eqn 1.2.4 ensures that the equation has a length scale, which is just $L = \sqrt{b/a}$. This simply means that we can make either the first or the second term on the right-hand side of Eqn 1.2.4 dominant, basically changing the balance of the equation towards the dimensions of the first or the second term. We refer to Eqn 1.2.4 as a *multiscale* equation. The length scale has been object of experimentation as well as theoretical analysis. In [53] the length scale is determined by comparing the response of two types of specimens, one in which the tensile softening damage remains distributed and one in which it localizes. In this scenario, the length scale is the ratio of the fracture energy, i.e. the energy dissipated per unit area to the energy dissipated per unit volume [53]. In the present paper, the length scale will be analyzed and identified with a fundamental parameter of peridynamics, called the horizon.

Chapter 2

Description of the computational model

The computational model used in the present work is based on peridynamics, a nonlocal theory in which integral equations replace differential equations. The peridynamics theory is explained in Section 2.1, while in Section 2.2 the implementation of peridynamics in a one-dimensional finite element framework is discussed.

2.1 Peridynamics

Peridynamics was introduced by Silling in 2000 [10] and draws its name from the Greek roots for *near* and *force*. Peridynamics was proposed as a framework for the basic equations of continuum mechanics useful when modeling discontinuities in materials, since the classical framework is not valid in such situations. The claim of the peridynamics theory is to be able to deal with discontinuities in a more direct and aesthetically pleasing way by employing integral equations and defining particles which can interact with each other in a strongly nonlocal model [10]. The underlying equations of peridynamics are going to be given in the present

section.

Suppose a body occupies a reference configuration in a region $\mathcal{R}$. It is assumed that each pair of particles interacts through a vector-valued function $\mathbf{f}$ such that $\mathbf{L}$, the force per unit reference volume due to interaction with the other particles, is a functional of the displacement field $\mathbf{u}$. At any time t and at any point $\mathbf{x}$ in the reference configuration, the value of $\mathbf{L}$ is given by [10]

$$\mathbf{L_u}(\mathbf{x},t) = \int_{\mathcal{R}} \mathbf{f}(\mathbf{u}(\mathbf{x}',t) - \mathbf{u}(\mathbf{x},t), \mathbf{x}' - \mathbf{x})\, \mathrm{d}V_{x'} \quad \forall \mathbf{x} \in \mathcal{R}, \quad t \geq 0, \tag{2.1.1}$$

which, if we avoid to write $\mathbf{u}$ as a function $\mathbf{x}'$, $\mathbf{x}$ and t, can be written more concisely as [10]

$$\mathbf{L_u}(\mathbf{x}) = \int_{\mathcal{R}} \mathbf{f}(\mathbf{u}' - \mathbf{u}, \mathbf{x}' - \mathbf{x})\, \mathrm{d}V' \quad \text{on } \mathcal{R}. \tag{2.1.2}$$

The *peridynamic equation of motion* is given by [10]

$$\rho \ddot{\mathbf{u}} = \mathbf{L_u} + \mathbf{b} \quad \text{on } \mathcal{R}, \quad t \geq 0 \tag{2.1.3}$$

and the *peridynamic equilibrium equation* is given by [10]

$$\mathbf{L_u} + \mathbf{b} = \mathbf{0} \quad \text{on } \mathcal{R}, \tag{2.1.4}$$

where $\mathbf{b}$ is the *loading force intensity*, i.e. the the external force per unit volume. In peridynamics the function $\mathbf{f}$ is called *pairwise force function* and it represents the backbone of the peridynamic theory. As mentioned in 1, no spatial derivatives appear in Eqn 2.1.2. It is important to note that in Eqn 2.1.2 the function $\mathbf{f}$ does not contain any history-dependent variable as argument, which means that the material described by this function does not have memory of its deformation history. Such a material is called *peridynamic material without memory* [10] and the terminology associated with it will become important in this paper because of its implementation in a quasi-static finite element code. The following notation is used throughout the paper for relative displacement vectors and relative position vectors in the reference configuration [10]:

$$\boldsymbol{\eta} = \mathbf{u}' - \mathbf{u} \qquad \boldsymbol{\xi} = \mathbf{x}' - \mathbf{x}. \tag{2.1.5}$$

Note that $\boldsymbol{\xi} + \boldsymbol{\eta}$ is the relative position of the particles in the deformed configuration. The direct physical interaction between the particles $\mathbf{x}$ and $\mathbf{x}$' is called *bond* in peridynamics [10].

Fundamental in the peridynamic theory is the concept of *horizon*. The horizon δ is a positive number such that [10]

$$|\boldsymbol{\xi}| > \delta \Rightarrow \mathbf{f}(\boldsymbol{\eta}, \boldsymbol{\xi}) = \mathbf{0} \quad \forall \boldsymbol{\eta}. \tag{2.1.6}$$

For the remainder of this discussion, $\mathcal{H}_{\mathbf{x}}$ will denote the spherical neighborhood of $\mathbf{x}$ in $\mathcal{R}$ with radius δ. Each point $\mathbf{x}$ in the body interacts directly with all the other points in the sphere $\mathcal{H}_{\mathbf{x}}$ through bonds and does not connect with points outside his horizon, as it is shown in Figure 2.1. The horizon is, therefore, a way to control the nonlocality of the model by choosing how many particles, or at what distance, we want these particles to interact [54] with each other. The peridynamic horizon can be viewed as an 'effective interaction distance' or an 'effective length scale' [54]. It will be explained later in the present work what values of δ were chosen to run the simulations, what values the literature suggests and how these values are chosen. There are theoretical ways one can go about to guess the value of the horizon: to treat is as a physical quantity, with a meaning in real life, and assign it a fixed length depending on the properties of the material being analyzed; or treat it as a computational quantity, with no meaning in real life, and assign it a value based on computational efficiency. In this last case the value, rather than being a fixed length, will most likely become a multiple of Δx, where Δx is the minimum distance between any two particles in the body. The physical meaning of the horizon can be searched in chemistry, where we know that atoms and molecules interact with each other over short distances, which though extend beyond the atom's nearest neighbours, especially in solid matter. In dynamic fracture, a way for particles to interact over a finite distance greater than the distance from the nearest neighbor is called *long range interaction* and was suggested by Ramulu et al [55, 56] and Streit and Finnie [57]. This criterion involves a 'characteristic distance r_o' that depends on the dynamic state of stress near the crack tip [54]. In [55] it is guessed that crack branching occurs when $r_0 \geq r_c$, where r_c is a material property related to the distance between microvoids and the crack tip. Hence, the concept of a length scale is not new, although its use in dynamic fracture was mostly related to branching and applied only near the crack tip. As it will be shown next, the horizon plays a role in the convergence of peridynamics towards classical mechanics or molecular dynamics.

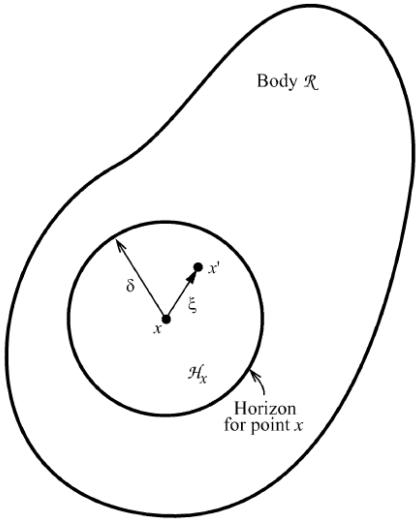

Figure 2.1: Graphical representation of the meaning of the horizon in a peridynamic body (from Ref [3]: Silling and Askari, "A meshfree method based on the peridynamic model of solid mechanics", *Computers and Structures*, 2005. Used with permission of Elsevier).

In [58] it is shown how the peridynamic model for an elastic material reproduces the classical model as δ goes to zero and m fixed, where m is the number of particles inside the horizon. This convergence is called δ-convergence. This is proven by collapsing the peridynamic stress tensor into the Piola-Kirchhoff stress tensor, given that the motion, constitutive model and any nonhomogeneities are sufficiently smooth. The Piola-Kirchhoff stress tensor is a function of the local deformation gradient tensor only, it is differentiable and its divergence represents the force density due to internal forces. Hence, the peridynamic model converges to the classical model if the horizon becomes infinitely small. A second type of convergence is called (δm)-convergence: δ decreases and m increases faster than δ decreases. In this case the numerical peridynamic approximation converges to the analytical peridynamic solution and converges uniformly to the local classical solution almost everywhere [59]. The last type of convergence in peridynamics is called m-convergence and is related to the number of particles taken into consideration inside a fixed horizon. As the number of particles is increased, in fact, peridynamics tends to the more complex and computationally expensive molecular dynamics, in which individual atoms are modeled and the potentials need to be known. As there is a huge

quantity of atoms and molecules to be analyzed even in the smallest piece of material, molecular dynamics can be seen as a downscaling of peridynamics, in which more information needs to be known and small defects and voids cannot be neglected. Figure 2.2 shows graphically what is meant by δ-convergence and m-convergence. At the end of the present section the similarities and the differences between peridynamics and molecular dynamics will be discussed, amongst other conclusions about peridynamics. In peridynamics,

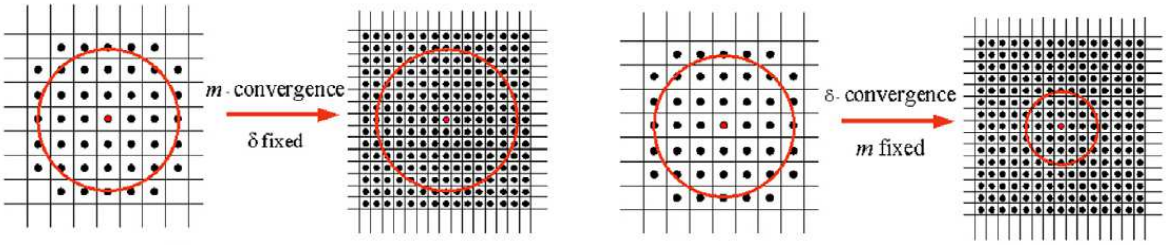

(a) m-convergence (b) δ-convergence

Figure 2.2: Schematic description of m-convergence and δ-convergence (from Ref [4]: Hu and Ha and Bobaru, "Peridynamic model for dynamic fracture in unidirectional fiber-reinforced composites", *Comput. Methods Appl. Mech. Engrg*, 2012. Used with permission of Elsevier).

because the body is not a continuum and is made of particles and voids, the concept of cross-sectional area is hard to define. Hence, the concept of traction as well is not directly understandable as it is in the conventional theory and needs to be redefined [10]. Suppose a plane $\mathcal{P}$ divides the body into two subregions $\mathcal{R}^+$ and $\mathcal{R}^-$. Then $\mathcal{R}^+$ exerts some forces on $\mathcal{R}^-$. This force is applied not just on the surface of $\mathcal{R}^-$, but through 'action of distance' (because of the nonlocality of the model) to particles below the surface as well. If this force is divided by the area of $\mathcal{P} \cap \mathcal{R}$, we have a notion of force per unit area. Defining $\boldsymbol{\tau}(\mathbf{x}, \mathbf{n})$ as the *areal force density* and skipping the mathematical derivation for summary purposes, we obtain [10]:

$$\boldsymbol{\tau}(\mathbf{x}, \mathbf{n}) = \int_{\mathcal{L}} \int_{\mathcal{R}^+} \mathbf{f}(\mathbf{u}' - \hat{\mathbf{u}}, \mathbf{x}' - \hat{\mathbf{x}}) \, \mathrm{d}V_{x'} \, \mathrm{d}\hat{l}, \tag{2.1.7}$$

where the hat ($\hat{}$) makes the different sets of points collinear and $\mathrm{d}\hat{l}$ represents the differential path over the length $\mathcal{L}$. As mentioned, the quantity defined in Eqn 2.1.7 is the closest thing to traction one can obtain in the peridynamic framework.

The boundary conditions in peridynamics need now to be discussed. In continuum mechanics, boundary conditions must be supplied to make the partial differential equations yield specific solutions in equilibrium problems. This happens because the differential equations model forces between particles that are in direct contact with each other; this creates a complete definition of how particles interact with each other inside the body; on boundaries, on the other hand, particles are not surrounded by other particles and need additional conditions that provide a complete description of their behavior. When the governing equations are derived from the potential energy functional, the condition of reaching a stationary state must be satisfied and the 'natural boundary conditions' (which define the force (or traction) of the particles at the boundary under consideration) appear automatically [10]. In the peridynamic theory, when deriving the governing equations, no natural boundary conditions emerge. Also, as discussed previously, no traction vector exists that has a natural function in the mechanics of the problem (the concept of areal force density was introduced as a way to compare the conventional theory to peridynamics). Hence, the concept of traction boundary condition does not apply to the present approach, where external forces must be supplied through the loading force density $\mathbf{b}$. These forces can be made nonzero depending on the loading mode that has to be analyzed, and are called *force loading conditions*. This approach resembles the finite element application of continuum problems, where loading boundary conditions are applied at some nodes, not on a volume (surface or line, depending on the dimensions of the problem). This characteristic of peridynamics simplifies its finite element implementation, because the loading force density $\mathbf{b}$ is very similar to the loading vector used in the finite element method. Displacement boundary conditions in continuum mechanics do have an analogue in peridynamics. Because there is no defined 'boundary' in peridynamics the analogue condition is called *displacement loading condition* and is defined as follows: we let $\mathcal{R}$ be the region in which Eqns 2.1.3 and 2.1.4 hold. We assume that in the complement of $\mathcal{R}$ there is another set of points $\mathcal{R}^*$, which are the particles in which the displacement is specified. In this scenario, the displacement field $\mathbf{u}^*$ is a vector field defined on $\mathcal{R}^*$. Now, points in $\mathcal{R}$ interact with points in $\mathcal{R}^*$ through the pairwise force function $\mathbf{f}$. Then, if

displacement loading conditions are present, the functional $\mathbf{L}$ in Eqn 2.1.2 becomes [10]

$$\mathbf{L}_{\mathbf{u}}(\mathbf{x}) = \int_{\mathcal{R}} \mathbf{f}(\mathbf{u}' - \mathbf{u}, \mathbf{x}' - \mathbf{x})\, \mathrm{d}V' + \int_{\mathcal{R}} \mathbf{f}(\mathbf{u}^* - \mathbf{u}, \mathbf{x}^* - \mathbf{x})\, \mathrm{d}V^*, \tag{2.1.8}$$

where $\mathbf{u}^* = \mathbf{u}^*(\mathbf{x}^*)$, $\mathrm{d}V^* = \mathrm{d}V_x$ was used and $\mathbf{L}$ is called *displacement load*. In peridynamics, the solution (displacement field) is satisfied automatically as the loading conditions are incorporated into the equations of equilibrium and motion. Because the loading conditions do not need to be applied separately, there is no need to talk about a displacement field that needs to satisfy the equilibrium equations and the boundary conditions [10]. Again, this way of defining the displacement loading conditions is very similar to what is used in the finite element method and Eqn 2.1.8 resembles a section of the weak formulation of a two-dimensional problem where the area integrals representing the body and the line integrals representing the boundaries where the displacements are known are separated and moved to opposite sides of the equation.

In [10] the stress tensor is found by comparing the result obtained using Eqn 2.1.7 to the deformation in the conventional theory of elasticity. It is shown that Poisson's ratio ν obtained for homogeneous deformations of linear isotropic materials can only assume the value of 1/4, which corresponds to what follows from the Cauchy relation for a solid composed of a lattice of points that interact only through a central force potential. There are ways to get around this limitation, such as adding an energy term that will take into account the movement of the electrons (especially in metals) in the derivation of the governing equation. Also, in [60] in 2007, a new formulation of the peridynamic theory, called *peridynamic states*, was introduced. In this new formulation some issues with the original theory are addressed: Poisson's ratio of 1/4; the fact that recasting a material model in terms of a pairwise force function becomes a practical barrier when using the peridynamic approach, because of the stress tensor description of the constitutive behavior in continuum mechanics; finally, plasticity cannot be adequately modeled because it results in permanent deformation of a material undergoing a volumetric strain (without shear), which is inconsistent with plastic incompressibility in metals. The peridynamic states formulation is not used in the present work but it is worth noting its importance in modeling a great range of materials. On the other side, as it will be discussed later, for a finite element application using one-dimensional bonds the fact that particles can only interact through a

central force potential is of help, since it makes the finite element formulation easy to obtain and converge to the well known case of a system of truss.

In peridynamics, a configuration is said to be *unstressed* if [10]

$$\boldsymbol{\tau}(\mathbf{x}, \mathbf{n}) = \mathbf{0} \quad \forall \mathbf{x} \in \mathcal{R}, \quad \forall \mathbf{n}. \tag{2.1.9}$$

The unstressed configuration for a given body can be obtained in two different ways: in the restrictive way the pairwise force between any two particles vanishes; in the second way, the pairwise force between any two particles is nonzero and actually significant. This second way to define an unstressed body is consistent with real materials, where the interatomic forces are always nonzero. Eqn 2.1.9 implies that the distribution of forces between particles, if it is nonzero, be repulsive (positive) for some values of interparticle distance and attractive (negative) for others. In the present work, because one-dimensional bar are used to represent the bonds between particles in the finite element implementation, the terms 'repulsion' and 'attraction' are substituted by 'tension' and 'compression'. To obtain a body in unstressed configuration the average of the forces on all the bonds needs to be zero, therefore a reference length of the bonds needs to be set such that if the reference length is greater than the distance between two particles, the force between them is attractive; on the other hand, if the reference length is smaller than the distance between two particles, the force between them is repulsive.

Finally, worth noting are the similarities between peridynamics and molecular dynamics. As previously said, when the number of particles inside a fixed horizon is increased the peridynamic method converges to molecular dynamics. LAMMPS, a molecular dynamics code, can be used to implement peridynamics just by making changes to the input file, as carefully explained in [61]. In [5] it is shown how peridynamics can be derived as an upscaling of molecular dynamics by the use of Higher-Order Gradient Models (HOG), as in both methods the force on a particle is computed by summing the forces from surrounding particles; basically, a PD model is an upscaling of an MD model if both produce the same HOG model [5]. A graphical representation of this concept is given in Figure 2.3. The solutions of MD simulations can most of the times be recovered by peridynamics. Along with these results, the paper also presents an analytical comparison of

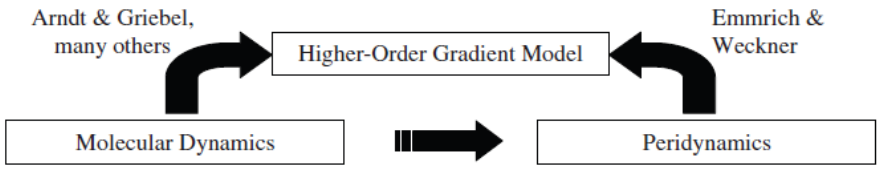

Figure 2.3: Connection between a molecular dynamics (MD) and a peridynamics (PD) model through a higher-order gradient (HOG) model (from Ref [5]: Seleson and Parks and Gunzburger and Lehoucq, "Peridynamic as an upscaling of molecular dynamics", *Multiscale Modeling Simulations*, 2009. Copyright ©2009 Society for Industrial and Applied Mathematics. Reprinted with permission. All rights reserved).

the equations of motion and dispersion relations for MD and PD to support the thesis of the authors. In [10] the PD model is referred to as a continuum formulation of MD, but in the same paper some important differences between the two theories are also stated: peridynamics is a continuum theory, in which the individual atoms need not be modeled and a physically correct interatomic potential need not be known [10]; second, in MD the interaction between particles is analogous to the structureless interactions described in the same paper (which describes peridynamic materials, in which the pairwise force function $\mathbf{f}$ depends only on the current position of the two particles), because particles (or atoms) have no memory of their position in any reference configuration, while peridynamics is able to handle materials not structurelss as well [10].

2.2 Finite Elements Implementation

In the present section the implementation of peridynamics in a finite element framework using one-dimensional bars to represent the bonds between particles is described. For consistency, the peridynamics particles will be called nodes and the bonds will be called bars, as that is what they represent. It is worth noting that the concept of a bond extending over a finite distance is a fundamental difference between the peridynamic theory and the classical theory, in which contact forces are the only way for two adjacent particles to communicate [11]. Because of this fundamental difference, the solutions found using the peridynamic truss model

in finite elements will lie on the length that connects two nodes, i.e. the bar; depending on the density of the nodes in the two-dimensional mesh, the solution will show voids or superposition of different bonds. The presence of voids and multiple bonds is due to the fact that a two-dimensional body is being approximated by a collection of massless particles connected by one-dimensional bonds. In Figure 2.4 a sample mesh made of 2274 nodes and 8686 truss elements is shown to give an example of how a 2-D plate is built using one dimensional truss elements.

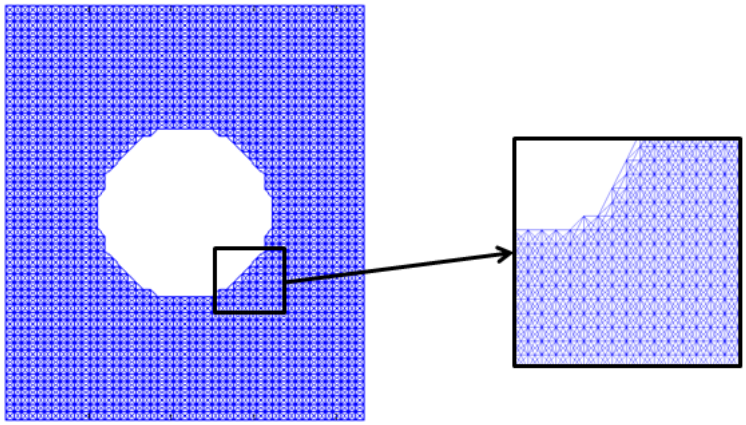

Figure 2.4: 2-D plate built using one dimensional trusses and detail.

We recall that, as developed in [3], the pairwise force for the basic theory can be written as

$$\mathbf{f}(\boldsymbol{\eta}, \boldsymbol{\xi}) = \frac{\boldsymbol{\xi} + \boldsymbol{\eta}}{|\boldsymbol{\xi} + \boldsymbol{\eta}|} f(y(t), \boldsymbol{\xi}, t) \quad \forall \boldsymbol{\xi}, \boldsymbol{\eta}, \tag{2.2.1}$$

where f is the scalar bond force and [3]

$$y = |\boldsymbol{\eta} + \boldsymbol{\xi}|. \tag{2.2.2}$$

We define the *scalar bond stretch* s as [3]

$$s = \frac{|\boldsymbol{\xi} + \boldsymbol{\eta}| - |\boldsymbol{\xi}|}{|\boldsymbol{\xi}|} = \frac{y - |\boldsymbol{\xi}|}{\boldsymbol{\xi}}, \tag{2.2.3}$$

which is identical to the engineering strain in the trusses. The micromodulus c corresponding to the classical continuum mechanics bulk modulus k is found simply by equating the strain energy under isotropic extension from continuum mechanics to the energy density within the horizon in the peridynamic theory for the same

deformation. Thus, from [3]:

$$c = \frac{18k}{\pi\delta^4} \tag{2.2.4}$$

while the critical stretch for band failure s_0 is related to the energy release rate G_0 by requiring the work to break all the bonds per unit area to equal the energy release rate [11], yielding

$$s_0 = \sqrt{\frac{10G_0}{\pi c\delta^5}} = \sqrt{\frac{5G_0}{9k\delta}}. \tag{2.2.5}$$

The materials analyzed in this paper are brittle with a yield/ultimate stretch s_y as it is shown in Figure 2.5. However, at the macroscopic level the material strain hardens because all bonds do not yield at the same time

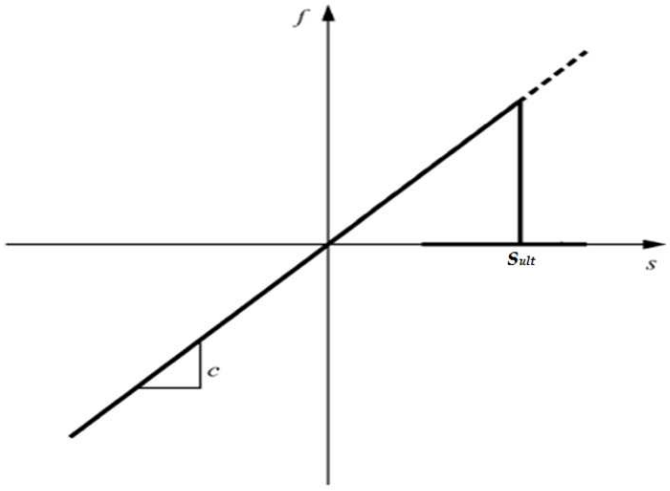

Figure 2.5: Bond force as a function of bond stretch in the present finite element model (from Ref [3]: Silling and Askari, "A meshfree method based on the peridynamic model of solid mechanics" *Computers and Structures*, 2005. Used with permission of Elsevier).

or deformation level [11]. Bond properties need to be related to the macroscopic properties of the material, so that real materials can be modeled following set relations. The ultimate stress σ_{ult} of the material can be related to the bond ultimate stretch by noting that all bonds have failed when the material reaches its ultimate strength. Other quantities will need to be analyzed and given physical sense in order to be able to understand the relations between macroscale properties and the properties of the individual bonds; among

these we have the horizon δ and the reference length of the bonds L_0.

The finite element implementation requires a mesh made of truss elements with the appropriate stiffness properties to represent the peridynamic bonds. Combining Eqn 2.1.2 and Eqn 2.1.4, discretizing the equation obtained and substituting the integral by a finite sum we obtain [11]:

$$\mathbf{0} = \sum_p \mathbf{f}(\mathbf{u_p^n} - \mathbf{u_i^n}, \mathbf{x_p^n} - \mathbf{x_i^n})\, V_p + \mathbf{b}_i^n, \tag{2.2.6}$$

where $\mathbf{f}$ is given in Eqn 2.2.1, n is the time step number and the subscripts denote the node number, so that [11]

$$\mathbf{u}_i^n = \mathbf{u}(\mathbf{x}_i, t^n). \tag{2.2.7}$$

Now, if we multiply Eqn 2.2.6 by V_i we obtain an equation of motion identical in form to that of FEA [11]:

$$\mathbf{0} = \sum_p \mathbf{f}(\mathbf{u_p^n} - \mathbf{u_i^n}, \mathbf{x_p^n} - \mathbf{x_i^n})\, V_p V_i + \mathbf{b}_i^n V_i, \tag{2.2.8}$$

which can be solved for the displacements.

Let's now just briefly recall the theory behind the analysis of truss structures in finite elements. Truss elements are 'two force members', loaded by two equal and opposite collinear forces which act along the line through the two connection points of the member. Truss members do not support bending moment, therefore can only stretch and compress axially. Cross sectional dimensions and elastic properties of each member are constant along its length, which is assumed to be much larger than its cross-section. Also, the force is constant along a truss member. Truss members can interconnect in space forming 1-D, 2-D or 3-D configuration, although the member itself only possesses one dimension [6], as it is shown in Figure 2.6 Their characteristics are very important in structural analysis since calculations can be greatly simplified by the use of truss members instead of, for example, beam members, which deform transversally and carry a rotation. Finally, a truss member is mechanical equivalent to a spring, since it has no stiffness against applied loads except those acting along the axis of the member [11]; the only difference, in this case, is the presence of a cross-sectional area, which has no meaning in a spring. This issue will be discussed later, as bonds between particles do not have a cross-sectional area as well since they have no volume. In this

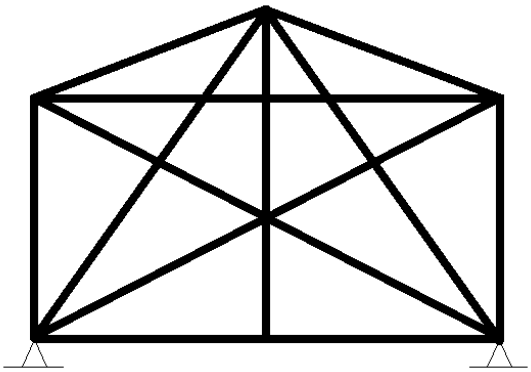

Figure 2.6: Complex trusses

work the terms 'truss member', 'truss' and 'bar' will be used interchangeably and will have the same exact meaning. The derivation of the finite element formulation starting from the equation of motion is skipped here and only the final result is given below. Eqn 2.2.9 shows [11]

$$\mathbf{0} = \sum_{p} \mathbf{f}(\mathbf{u_p^n} - \mathbf{u_i^n}, \mathbf{x_p^n} - \mathbf{x_i^n})\, V_p V_i + \mathbf{b}_i^n V_i, \tag{2.2.9}$$

which is in the classical form used by FEA. The governing equation of a bar can be obtained from equilibrium and its matrix formulation element-wise is

$$\mathbf{K}^e \mathbf{u}^e = \mathbf{F}^e, \tag{2.2.10}$$

where the superscript e means that the matrices are written for a single truss element. Expanding in two dimensions we obtain

$$\mathbf{K}^e = \frac{E^e A^e}{L^e} \begin{bmatrix} c^2 & cs & -c^2 & -cs \\ cs & s^2 & -cs & -s^2 \\ -c^2 & -cs & c^2 & cs \\ -cs & -s^2 & cs & s^2 \end{bmatrix}, \tag{2.2.11}$$

where c and s stand for *cosine* and *sine* of the angle of the bar. The vectors

$$\mathbf{u}^e = \begin{bmatrix} u_{1x} \\ u_{1y} \\ u_{2x} \\ u_{2y} \end{bmatrix} \tag{2.2.12}$$

and

$$\mathbf{F}^e = \begin{bmatrix} F_{1x} \\ F_{1y} \\ F_{2x} \\ F_{2y} \end{bmatrix}, \tag{2.2.13}$$

are also defined, where the subscripts 1 and 2 stand respectively for node 1 and node 2, while the subscripts x and y represent the degree of freedom of the nodes, respectively in the horizontal and in the vertical direction. In Eqn 2.2.10 we can solve for the displacement vector $\mathbf{u}^e$ to find the deformation in the horizontal and vertical directions.

In peridynamics the parameter for bond failure is displacement: when a particle falls out of the horizon of another particle, the strength of the bond between them goes to zero. In our case, the stiffness of the bar goes to zero, making the truss member between two particles disappear. In the present work the stretch of the truss member between two particles is taken a second parameter for failure, such that the stiffness of the member goes to zero as the strain along it overcomes a maximum value, which needs to be chosen either computationally or analytically. The procedure of finding the ultimate stretch will now be explained. Once Eqn 2.2.10 is solved for the horizontal and vertical displacements of each node, we need to find the actual elongation each bar has gone through, which requires the knowledge of the geometry of the problem. The

actual elongation of each bar u_n^e is found by

$$u_n^e = \begin{bmatrix} -c & -s & c & s \end{bmatrix} \begin{bmatrix} u_{1x} \\ u_{1y} \\ u_{2x} \\ u_{2y} \end{bmatrix}. \tag{2.2.14}$$

Once the value of u_n^e is obtained we need to account for the reference length L_0 of the bar. L_0 is the original (unstretched) length of the bar, such that, at time $t = 0$, some bars will be in tension and others will be in compression. This is fundamental for the average of the stress on all the bars will need to be equal to zero for the body as a whole to be initially unstressed, while the individual bars will be stretched and compressed, depending on the distance between any two particles. The quatity L_0 also carries a physical meaning with it, because the bonds between molecules and atoms do have reference lengths that allow them to stay in equilibrium in an 'unstretched' macroscale reference configuration. In the present work the value of L_0 is chosen computationally by looping the initial part of the code until the average stress of all the bars in the body is as close as possible to zero in the reference state. This is shown in Figure 2.7. Furthermore, L_0 is

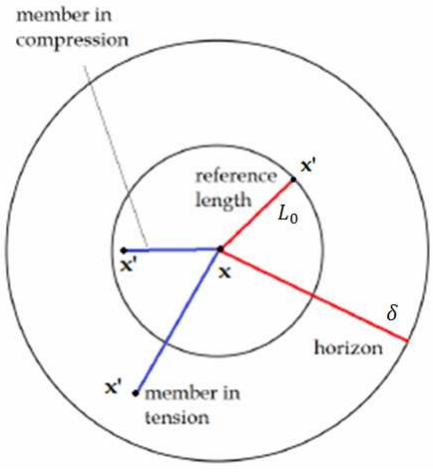

Figure 2.7: Scheme representing the meaning of the reference length in the reference configuration.

found to depend on the number of nodes and the value of the horizon δ. Once the reference length of the

bars is decided, we need to find the new elongation by

$$u^e_{n,new} = L^e - L_0 + u^e_{n,old}. \tag{2.2.15}$$

From now on, we will just use $u^e_{n,new}$ and we will omit the *new* subscript. Finally, the constitutive relations needed to find the stress along a bar are given below:

$$\epsilon^e = \frac{u^e_n}{L^e}, \tag{2.2.16}$$

where ϵ^e is the strain, u^e_n is the displacement of the nodes of the bar and L^e is the length of each bar. Because $\sigma = \epsilon E$, the constant stress on a bar is found by

$$\sigma^e = \frac{E^e}{L^e} u^e_n. \tag{2.2.17}$$

The mesh generated in the present work is a uniform rectangular mesh, which simplifies the expressions for the cross sectional area and the Young's modulus of the truss bar. The definition of cross-section and material properties for the peridynamic trusses is a straightforward application of the theory. Because Eqn 2.2.9 indicates that only the forces from the trusses connected to a given node are required, the definition of the cross-sectional area A and elastic modulus E for the trusses is somehow non-unique [11]. A convenient separation, which preserves the conventional units of these properties, is [11]

$$A = \Delta x^2, \qquad E = c\Delta x^4. \tag{2.2.18}$$

where Δx is the minimum distance between any two nodes in the mesh. Also, as shown in Eqn 2.2.3, the bond stretch s is identical to the engineering strain in the trusses, therefore the fracture strain of the trusses is [11]

$$\epsilon_f = s_{ult}. \tag{2.2.19}$$

For elastic-plastic materials, Eqn 2.2.9 with the inherent Poisson's ratio of 1/4 indicates that the strain s_{ult} at which the bonds or trusses fail is related to Youngs modulus E and the engineering ultimate stress in tension σ_{ult} by [11]

$$s_{ult} \approx \frac{\sigma_{ult}}{2E} \tag{2.2.20}$$

For FEA implementation, we set the truss element yield strain to $\varepsilon_f = s_{ult}$ as determined by Eqn 2.2.20 [11]. The horizon of length $\delta = 3\Delta x$ is shown to work well for macroscale modeling, as much smaller values result in crack growth along the rows or columns of the grid, while bigger values result in excessive wave dispersion and become too computationally expensive [11].

The simulations run and depicted in the present work are quasistatic. Quasistatic integration schemes are typically employed to alleviate the stringent time step restrictions imposed by explicit time integration schemes [62]. However, this simplification carries with it the downside of not being able to account for stress waves, which are often important in fracture problems since they have affect the stress distribution in the body. Despite this issue, quasistatic simulation are very consistently employed in damage analysis and the effects of stress waves is often ignored in order to focus on other computational issues that do come up in this kind of simulations. In the present work, we will assume that strain is applied to the material very slowly, so slowly that the body is always in equilibrium and reaches stationary state at every time step. This assumption usually comes in handy when taking the process as isotropic, meaning that no energy is dissipated and that the process is reversible; this is only the case as long as fracture is not achieved; once fracture happens the body is not supposed to come back together as it was before, meaning that the process is not reversible. With fracture, it is implicity assumed that energy is dissipated in some other ways, such as heat.

Chapter 3

Results and Discussion

In the present chapter some results obtained implementing peridynamics in finite element will be compared to the same cases in regular bond-based peridynamics from literature, subsequently, two rectangular plates will be analyzed, with a hole and with a fiber inclusion, will be analyzed and their stress distributions will be discussed and compared to the analytical solution. Under different boundary conditions these samples will be brought to fracture and the damage will be analyzed and compared to the solution of a finite element code with cohesive zone. The samples are classical RVEs (Representative Volume Elements) with width/height $= \sqrt{3}/2$; finally, a qualitative study on three hexagonal RVEs undergoing fracture will be presented to show how peridyamics can be applied to this category of problems.

3.1 Comparison with a 2D computational peridynamics implementation

In the present section the results for a plate with a hole in tension obatined using the implementation of peridynamics with truss elements will be compared to the results obtained using bond-based peridynamics

as applied using a different 2D numerical implementation. The results are from a 2011 paper by Bobaru and Ha [63]. The plate considered is a square with a side of 6 cm and a hole in the center of 5 mm in radius; a traction of 10 MPa is applied to the right and left sides. The material has a Young's modulus of 1 GPa. The horizon was set at 4 mm, which corresponds to about $4\Delta x$, while the micromodulus used in [63] is conical. Figure 3.1 shows good agreement between the numerical solutions. The behavior is similar, stress concentrates in the right areas and the magnitude of the displacements is close in most of the surface.

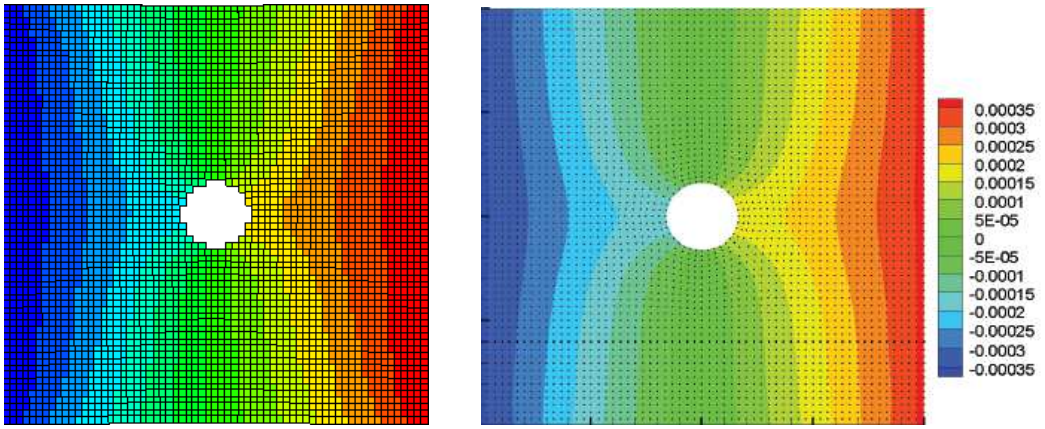

(a) u_x in truss peridynamics (m).

(b) u_x in 2D peridynamics (m) (from Ref [63]: reprinted from *International Journal for Multiscale Computational Engineering*, Vol. 9, Bobaru and Ha, "Adaptive refinement and multiscale modeling in 2D peridynamics", pp.635-660, Copyright ©2011, with permission from Begell House, Inc.).

Figure 3.1: Truss-implemented peridynamics and 2D peridynamics solution for u_x.

The results for u_y shown in Figure 3.2. Unlike Figure 3.1, the result obtained using truss-based peridynamics are not in perfect agreement with the ones obtained in [63] using a 2D implementation. The behavior of the solution, especially as we go further away from the center hole, diverges from the 2D peridynamics solution. Despite this incongruence, Figure 3.1 and 3.2 show promising results since it seems that truss-based peridynamics can be a further method to translate the peridynamic theory into computation, adding

tools for the modeling of solids undergoing stress or frature, hence giving different ways to compare the results obtained.

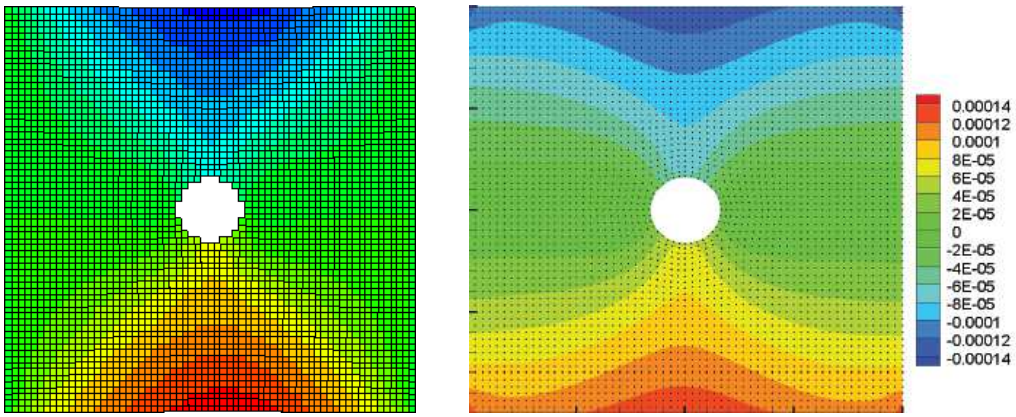

(a) u_y in truss peridynamics (m).

(b) u_y in 2D peridynamics (m) (from Ref [63]: reprinted from *International Journal for Multiscale Computational Engineering*, Vol. 9, Bobaru and Ha, "Adaptive refinement and multiscale modeling in 2D peridynamics", pp.635-660, Copyright ©2011, with permission from Begell House, Inc.).

Figure 3.2: Truss-implemented peridynamics and 2D peridynamics solution for u_y.

3.2 Plate with a hole in the center

3.2.1 Stress analysis

The first case discussed is an aluminum plate ($E = 70$ GPa) with a hole in the center. The analytical solution was found using Airy stress function as described in [64] for an infinite plate in tension with a traction of 10 GPa applied at the top and bottom sides. As described in Section 2.2, the finite element implementation of peridynamics in this paper allows only one elastic constant, the micromodulus c given in Eqn 2.2.4, whereas isotropic linear elastic materials in the classical theory (such as aluminum) are characterized by two such

constants [11]. This difference occurs because an elastic solid that involves only two-particle interactions (called "Cauchy crystal") always has a Poisson ratio of 1/4. Hence, in finding the analytical solution a Poisson ratio of 1/4 (instead of 0.35) is used to be consistent with the results found using peridynamics. For consistency, the displacement functions are obtained using Airy stress function for an infinite plate in tension and are applied to the boundaries of the RVE in the peridynamic code, to make sure the same the same loading case is being analyzed. The results obtained for u_y, u_x, σ_{yy} and σ_{xx} (where x and y are respectively in the horizontal and vertical directions) are compared to the analytical solution and good agreement is found in both magnitude of displacements and stresses, as well as general behavior of the plate under tension. The mesh used in this simulation is a regular grid of 5784 equally spaced nodes, with a a horizon of $3\Delta x$, which bring the total number of truss elements to 77384. Δx is about 1.2% of the height of the sample and the reference length L_0 is found by iteration to be about 0.61δ. Cross sectional area and Young's modulus of the trusses are calculated following Eqn 2.2.18. The results are shown in Figure 3.3, 3.4, 3.5 and 3.6. In Figure 3.3 there is good agreement between the analytical solution and the result obtained using peridynamics, whereas in Figure 3.4 the displacements in the x-direction obtained using peridynamics are smaller in magnitude than in the analytical solution. To resolve this issue, different material properties were tried, as well as different Poisson ratios and horizons lengths: none of these patches had success in solving this issue, which then seems not to be dependent on the nonlocality of the model. An increase in the density of the mesh did not increase the accuracy of the model noticeably, while increasing computational time exponentially. A possible explanation, which will be given when discussing Figure 3.5 and 3.6, is the absence of a normalization factor for the elastic modulus of the trusses near the boundaries [11].

The need of a more refined mesh becomes obvious when looking at Figure 3.5, where the dimensions of each node are observable and the plot is not as smooth as desired. Unfortunately more refined meshes increased the computational time to several hours or caused the computer to crash, hence could not be performed for the present work. The machine used has a single CPU at 2.40GHz and 6GB of RAM. Although the implementation of peridynamics in a finite element code performed in the present work seems to be able

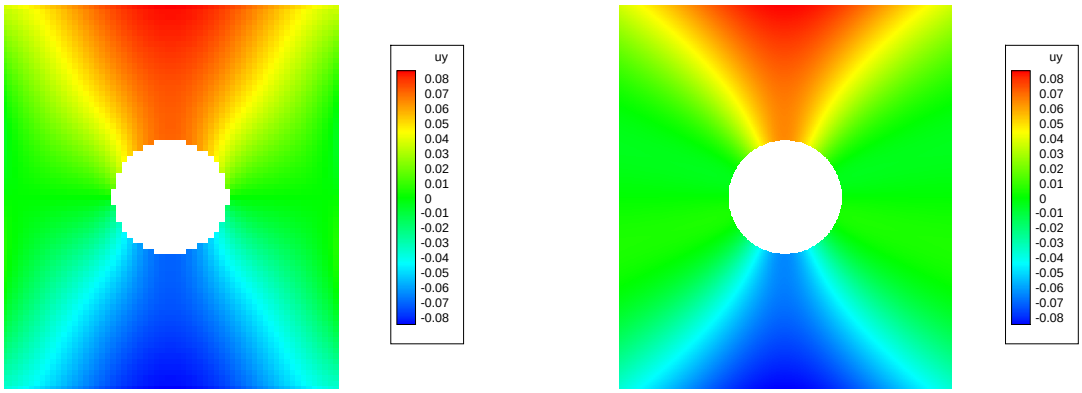

(a) u_y in peridynamics (m)

(b) u_y in analytical solution (m)

Figure 3.3: Peridynamics and analytical solution for u_y.

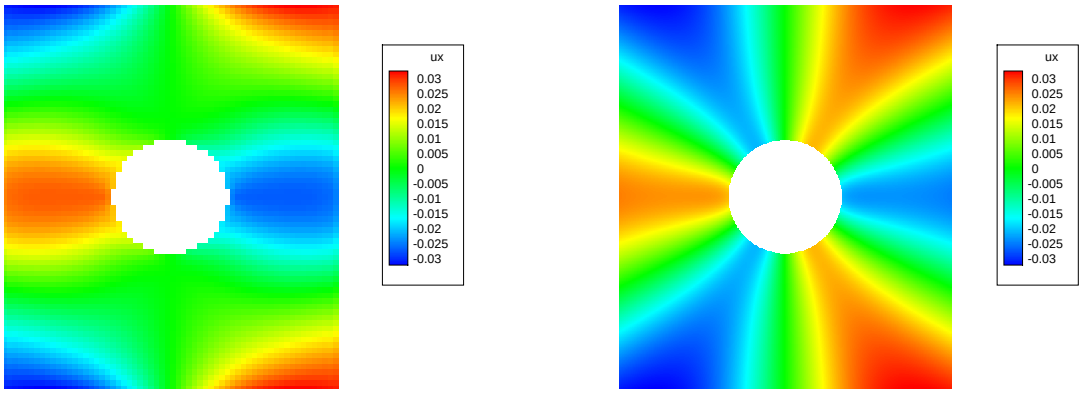

(a) u_x in peridynamics (m)

(b) u_x in analytical solution (m)

Figure 3.4: Peridynamics and analytical solution for u_x.

to give qualitatively good results, a much greater number of nodes, leading to an exponentially greater number of trusses, should be modeled to obtain smooth and more accurate results. This is particularly true near the hole at the center of the plate, where a regular rectangular grid is not sufficient if all the geometrical properties need to be modeled with great accuracy. As it is discussed in [11], peridynamics in finite elements is still much computationally cheaper than molecular dynamics or other meshless methods when comparable results are obtained. Nonetheless, the result for σ_{yy} shown in Figure 3.5a is in good agreement with the analytical solution given in Figure 3.5b both qualitatively and quantitatively, excluding the external boundaries of the sample and the free surface at the hole in the center. In these locations a normalization factor for the elasticity modulus should be used to account for the fact that nodes close to a free surface have a smaller connectivity than the internal ones, meaning that the stress calculated from the contribution of the trusses inside the sample is not balanced. This normalization factor needs to be calculated for every single truss element belonging inside the horizon of all the nodes close to a free surface and this made it too computationally expensive to implement; hence the stiffness of the plate near the boundary is higher than it should be and this can have affected both the displacements and the stresses. Figure 3.6a and Figure 3.6b show discrepancy near the boundaries due to the lack of a normalization factor, which makes the stress near the top and bottom free surfaces too high compared to the analytical solution. In future works this inaccuracy of the present simulations can be fixed by enriching the model with the normalization factor, although a more powerful machine is needed to run this simulations.

3.2.2 Fracture analysis

Now the efficacy of the peridynamics theory when modeling fracture is discussed. For this simulation the mesh is kept as a regular grid with 725 nodes and 2669 truss elements, with a maximum spacing between nodes Δx of 3% of the height of the sample. The horizon is $\delta = 3\Delta x$ and $L_0 = 0.6\delta$, while the total number of trusses is 1870. The maximum stretch of the bonds is found using Eqn 2.2.20, with $\sigma_{ult} = 24$ MPa. The bond stretch failure criterion is used in addition to the horizon criterion in determining whether a bond must

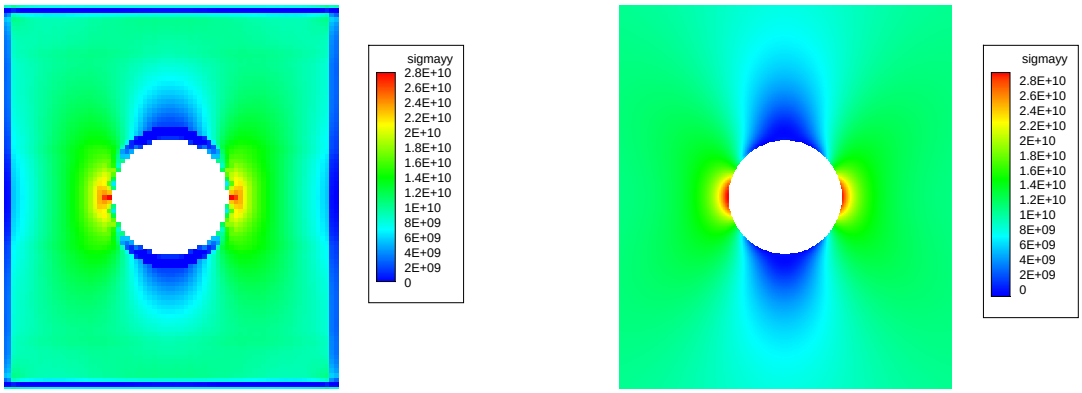

(a) σ_{yy} in peridynamics (Pa) (b) σ_{yy} in analytical solution (Pa)

Figure 3.5: Peridynamics and analytical solution for σ_{yy}.

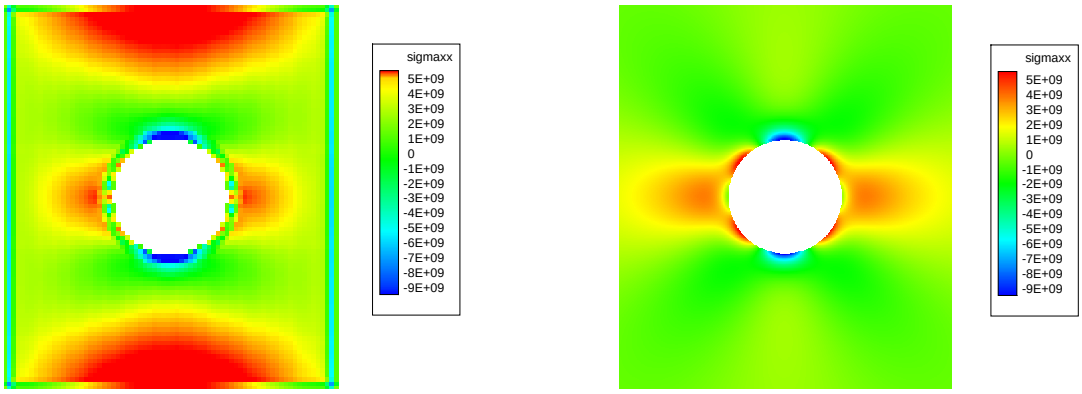

(a) σ_{xx} in peridynamics (Pa) (b) σ_{xx} in analytical solution (Pa)

Figure 3.6: Peridynamics and analytical solution for σ_{xx}.

be deleted: if the strain on an element becomes higher than the critical bond stretch or a node falls outside of the horizon of another node, that bond will be deleted and will not have further use in the simulation. The radius is increased to 0.2 times the height of the sample and tension is applied to both the top and bottom sides of the sample. Because this is a quasi-static simulation, the concept of time step is not relevant. The evolution of the crack is obtained by applying an incremental ϵ of 0.0005 at each step until complete fracture is achieved. In the simulation shown in Figure 3.7 145 steps are performed until an applied strain of 7.25% is reached at each end. The crack seems to form in the right location, starting from the hollow section and spreading to the sides of the sample, which agrees with observation and experimental results. Being the mesh so regular there is no changing direction of the crack which behaves in a very predictable way; to be able to increase the strain gradually and perform many steps in the calculations the number of nodes had to be reduced not to become too computationally expensive. The low density of nodes makes the simulation somehow mesh-dependent: the fact that some nodes detach from the main body can be due to this issue. In this simulation peridynamics seems to be able to predict the formation of a crack which happens naturally, without knowledge of its behavior in advance and without having to adjusting the mesh accordingly. Because of the discrete formulation and the interaction of the nodes through bonds the stresses and the energy are transfered effortlessly through the mesh and crack happens as a consequence of this process.

In Figure 3.8 the average stress in the bonds is plotted against the applied stress at the top and bottom sides for the fracture case descripted above. The plot starts negative because the reference length of the bonds is slightly too large, making most bonds be in compression at time zero. Because of the high stress present in the plate it is very computationally expensive to find a reference length which will make the plate be at exactly zero stress in the reference configuration; hence, the value found here was as close as possible to zero for this problem. The plot shows a linear elastic behavior of the stress-strain plot, which is expected; also, once fracture starts happening, the stress curve starts decreasing and pointing downwards, since many bonds are broken and not able to withstand load.

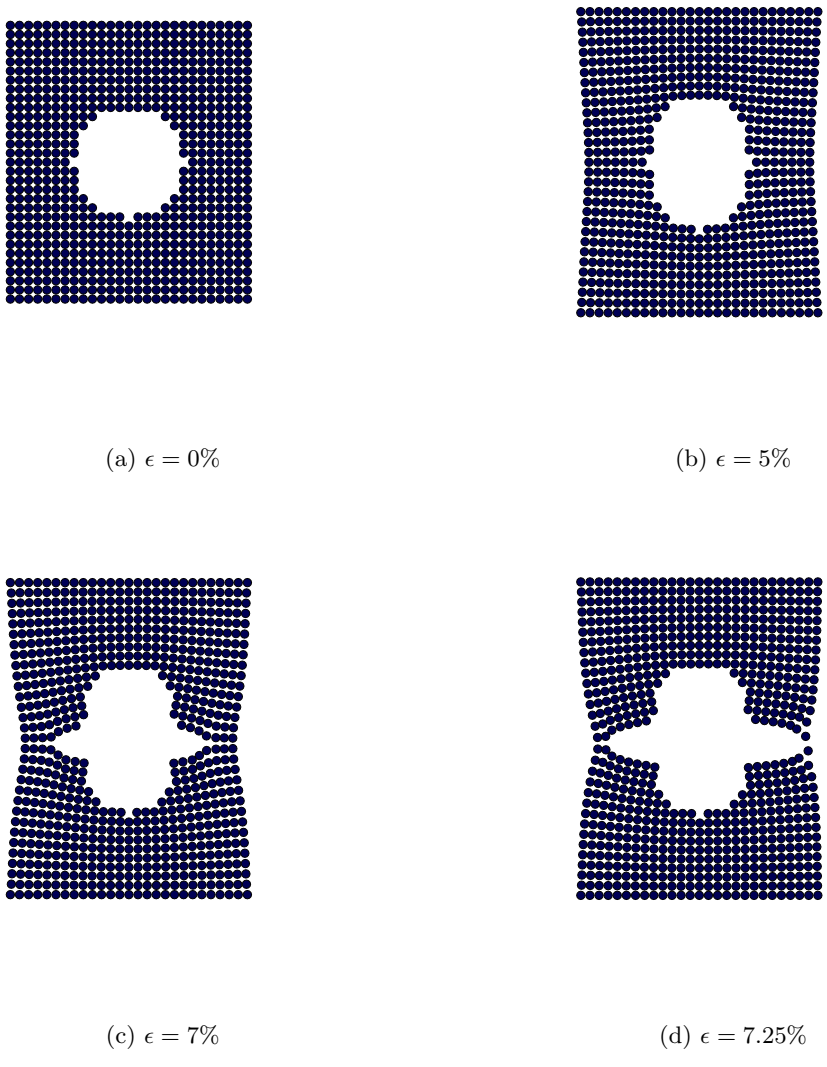

(a) $\epsilon = 0\%$

(b) $\epsilon = 5\%$

(c) $\epsilon = 7\%$

(d) $\epsilon = 7.25\%$

Figure 3.7: Damage propagation in hollow RVE using peridynamics.

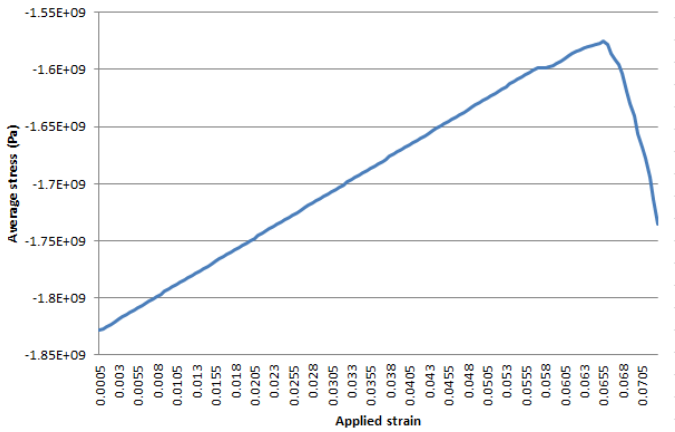

Figure 3.8: Average stress of the bonds against applied strain at the sides.

3.3 Plate with a fiber inclusion

3.3.1 Stress analysis

The second case discussed is a composite plate made of two phases. The mechanical properties of the materials are taken from [9]. The matrix is made of EPON 862 ($E = 3.07$ GPa) while the inclusion is made of a very stiff carbon fiber ($E = 898$ GPa). For simplicity, the materials are assumed to be isotropic even though this is not true for the carbon nanotube, which has a much lower transverse stiffness; also, Poisson ratio for both materials is still assumed to be 0.25. The analytical solution was found using Airy stress function for a plate in tension with a traction of 100 MPa applied to the top and bottom sides and the displacement functions at the boundaries were obtained and applied to the peridynamics code to link the infinite plate and finite plate cases. Again, the mesh is a regular grid made of 4402 nodes with a maximum spacing between nodes of about 1.5% of the height of the sample, $\delta = 3\Delta x$ and $L_0 = 0.61\delta$, which gave the lowest possible average stress in the reference state. In total, 59252 truss elements are used. The main issue with this simulation is the presence of more than one material in the RVE, which calls for a different definition of the bonds that extend from one phase of the composite material to the other. A graphical representation is given in Figure 3.9. Furthermore, the elastic moduli of the matrix and the inclusion differ

by two orders of magnitude, which means that what happens at the interface is critical but also difficult to model because more subject to great variation. Finally, since we are considering the mechanical properties of a carbon nanotube which has a radius of the order of a few nanometers, the problem involves the analysis of a nanocomposite, issue that is currently subject to a great amount of research and that requires very specific tools. In the present work, the stiffness of the bonds between particles both in the matrix or both in the inclusion were calculated following Eqn 2.2.18, while the Young's modulus of the bonds that connect a node in the matrix to a node in the inclusion was chosen to be an average of the two, 500 GPa. Other values for the interface elements were tried to simulate a weak (3.07 GPa), a strong (900 GPa) and a very strong (4000 GPa) interface, to attempt to replicate the perfect bonding case given in the analytical solution: the solutions obtained had more error and were farther away from the analytical solution than the case considered here, the 'medium strength' interface; hence, the simulations carried out in this thesis use a value of 500 GPa for the interface elements, i.e. those bonds that extend across the two different phases of the RVE.

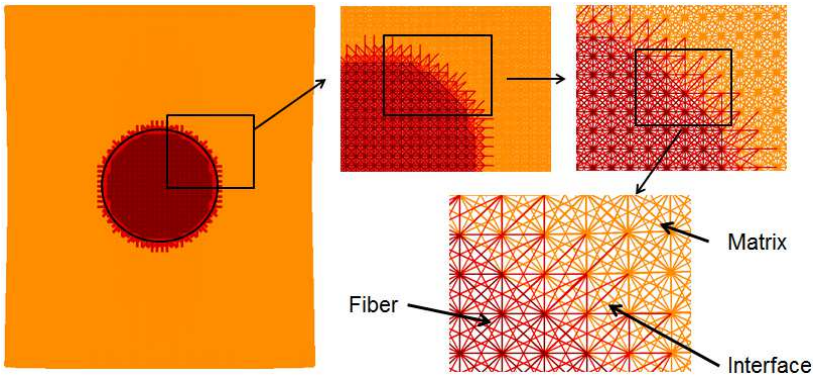

Figure 3.9: Graphical representation of interface truss elements.

As in Section 3.2, the displacements and the stresses are plotted. The displacements, shown in Figure 3.10 and 3.11, are in good agreement at the boundaries (which is expected since displacement boundary conditions are applied) but start diverging as we move closer to the inclusion. This can be due to the stiffness chosen for the interface elements or to the elastic modulus of the elements near the boundaries, too high because of the lack of a normalization factor. Refining the mesh had little to small success in improving the quality of the

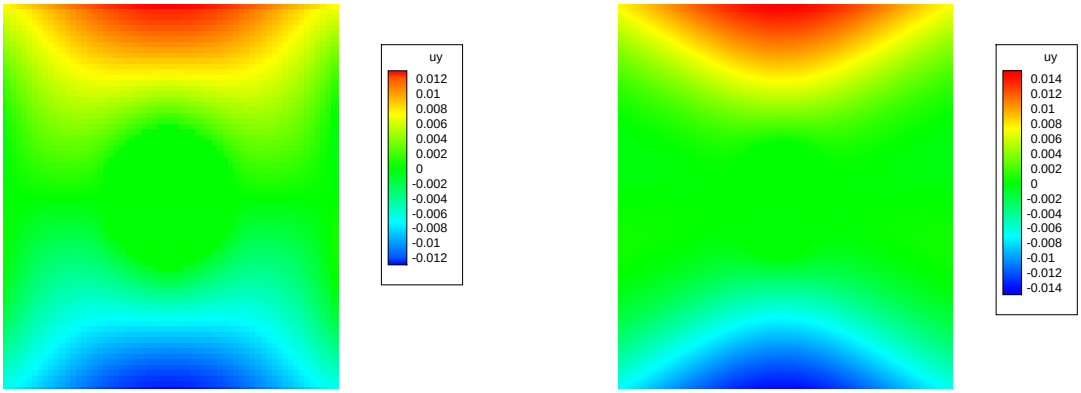

(a) u_y in peridynamics (m) (b) u_y in analytical solution (m)

Figure 3.10: Peridynamics and analytical solution for u_y.

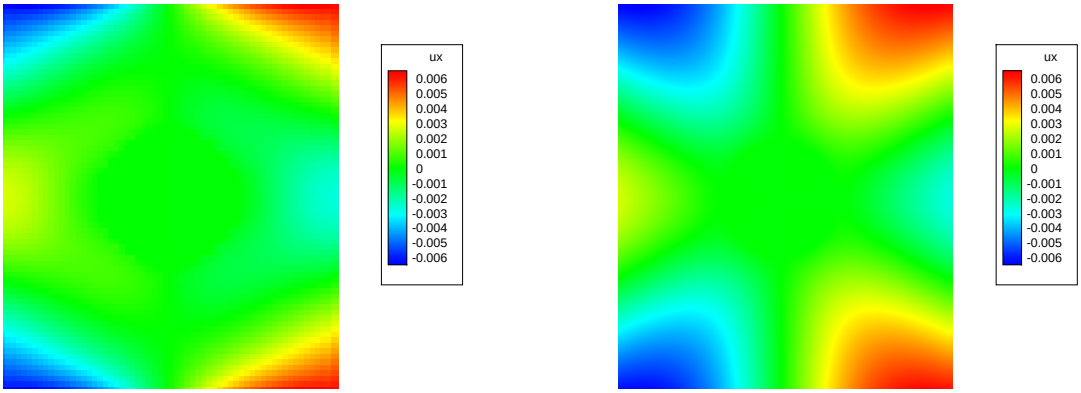

(a) u_x in peridynamics (m) (b) u_x in analytical solution (m)

Figure 3.11: Peridynamics and analytical solution for u_x.

solution, therefore the number of nodes was kept at 4402 to make sure the simulation would run smoothly on the computer.

The calculation of the stresses appears to be off compared to the analytical solution. A disturbance of the

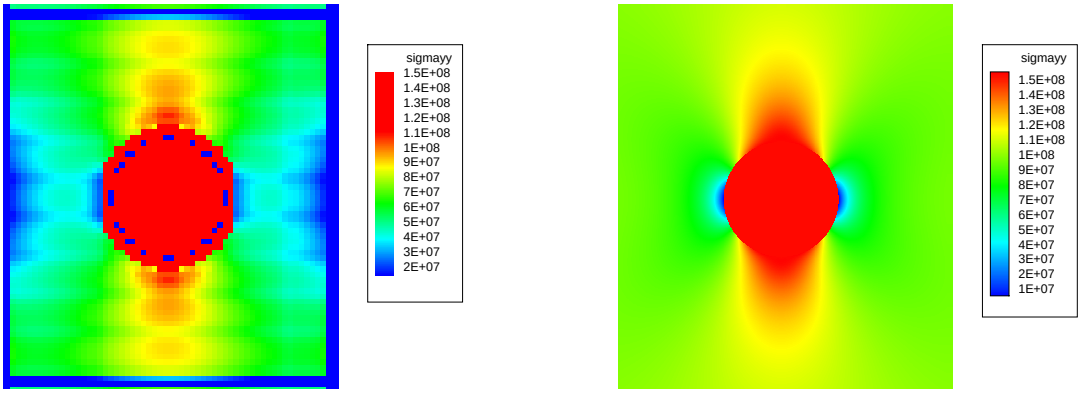

(a) σ_{yy} in peridynamics (Pa) (b) σ_{yy} in analytical solution (Pa)

Figure 3.12: Peridynamics and analytical solution for σ_{yy}.

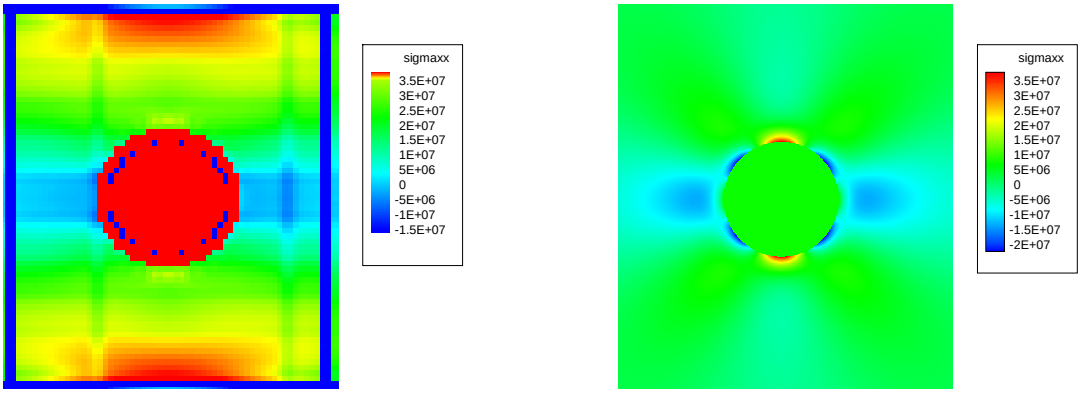

(a) σ_{xx} in peridynamics (Pa) (b) σ_{xx} in analytical solution (Pa)

Figure 3.13: Peridynamics and analytical solution for σ_{xx}.

form of a high-frequency oscillation is present in both σ_{yy} and σ_{xx} and can be seen in Figure 3.12 and 3.13. The cause of this disturbance is unknown. The magnitude of the stresses is for the most part in good agreement with the analytical solution if we exclude the areas near the left and right sides in σ_{yy} and the areas near the top and bottom sides in σ_{xx}, still due to the lack of a normalization factor. A different

argument must be made for Figure 3.13a, which reports a strangely high horizontal stress inside the inclusion. The causes of this discrepancy are hard to find and can be searched in the not very dense mesh, especially near the inclusion where more accuracy is needed, in the disturbance represented by two vertical lines, not symmetric, present in the RVE, or in the definition of the bonds and the nonlocality of the theory when dealing with different materials. In fact, the nodes (or particles) in the plate are interacting with each other inside the horizon even if the horizon extends outside the phase of the reference node and the stiffness of the elements is arbitrarily chosen to be the average of the moduli of the matrix and the inclusion. The same horizon was used for both materials, which is not said to be necessarily true. For future works a different definition of nonlocality might be implemented, in which nodes inside the inclusion interact with nodes inside the matrix following a different law or different computational restrictions.

3.3.2 Fracture analysis

Now propagation of fracture will be studied in the composite plate under tension. The mesh is kept as a regular grid with 837 nodes and a maximum spacing between nodes Δx of 3% of the height of the sample. The horizon is $\delta = 3\Delta x$ and $L_0 = 0.62\delta$, while the total number of trusses is 3176. The maximum stretch of the bonds is found using Eqn 2.2.20, where σ_{ult} for the EPON matrix is 100 MPa, while σ_{ult} for the CNT inclusion is taken to be 100 GPa [9]. The radius is 0.15 times the height and tension is applied to both the top and bottom sides of the sample. The evolution of the crack is obtained by applying a ϵ of 0.001 at each step until fracture is spread. In the simulation shown in Figure 3.14 119 steps are performed until an applied strain of 11.9% is reached at each end. Figure 3.14 shows the behavior of the composite material under these loading conditions. Because the yield strength of the CNT inclusion is three orders of magnitude higher than the yield strength of the matrix, the stress concentrates at the interface, more specifically at the lower and upper sides of the interface between the two materials. This happens because the particles in the matrix displace much more while high the elastic modulus of the trusses in the CNT keeps them almost fixed. Furthermore, this displacement means that the truss element yield strain is exceeded, causing the deletion

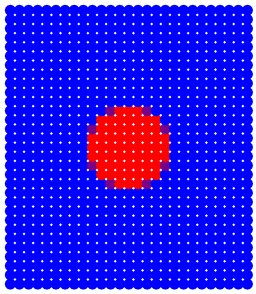

(a) PD finite element with $\epsilon = 0\%$

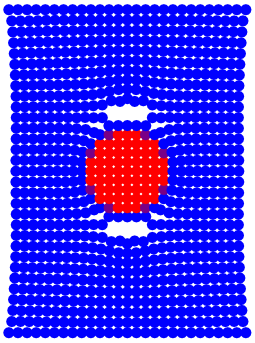

(b) PD finite element with $\epsilon = 9\%$

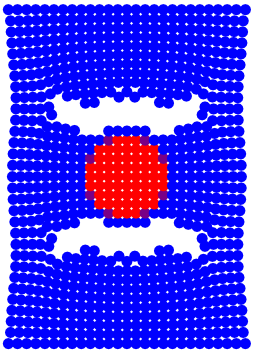

(c) PD finite element with $\epsilon = 11\%$

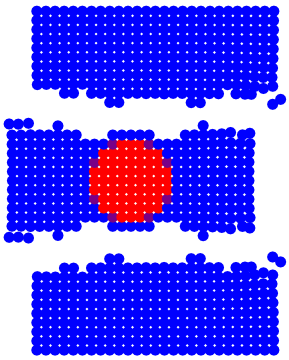

(d) PD finite element with $\epsilon = 11.9\%$

Figure 3.14: Damage propagation in RVE with inclusion using PD

of the trusses. This fracture mode is called debonding and, once it develops between the inclusion and the matrix it starts spreading horizontally until it eventually reaches the sides of the RVE being analyzed. This behavior is expected and is confirmed by observation and by a cohesive zone finite element (CZFE) code run for this particular case, as shown in Figure 3.15a and 3.15b. The solution obtained using the cohesive zone method shows that debonding happens as predicted and in a similar fashion to what obtained using peridynamics. The mesh of the CZFE code is denser, which makes the solution more accurate. Peridynamics seems to be able to predict crack evolution and the correct fracture mode naturally, without inputs on how or where cracks should form, which is opposite to the cohesive zone model, where spring elements are placed between 2-D mesh elements in the strategic points where it is thought crack is going to form and propagate. This happens in peridynamics spontaneously and it is a very encouraging fact the pushes us towards a deeper study of this theory.

(a) Cohesive zone finite element with $\epsilon = 0\%$ (b) Cohesive zone finite element with $\epsilon = 7.5\%$

Figure 3.15: Damage propagation in RVE with inclusion using CZFE

3.4 Hexagonal RVE

3.4.1 Fracture analysis

In this section the qualitative behavior of RVEs with different volume fractions and different interface elements stiffness will be studied when the sample is put under a tensile load. The material properties are the same used in Section 3.3. The mesh is made of 2707 randomly arranged nodes, which end up connecting about 30,000 elements within a horizon $\delta = 3\Delta x$, where $\Delta x = 2\%$. The reference length L_0 is about 0.58δ.

The first case studied is a hexagonal RVE with a volume fraction $V_f = 10\%$ and an interface elements stiffnes of 500 GPa. The ultimate toughness of the interface elements is 100 GPa, the same as the one used for the fiber inclusion. The plate is in tension, with and applied $\epsilon = 0.001$ at the top and bottom sides until a final strain of 5.3% is reached. Figure 3.16b shows how damage happens spontaneously in the form of debonding between three fibers and the matrix, while a crack initiates in the middle of the RVE on the right side. In Figure 3.16c and 3.16d the fractures propagate naturally until they almost join each other and the sample is about to break. Crack initiation, debonding and propagation happen naturally, with no need for additional parameters or preliminary information on how the sample is going to break. Damage happens as expected, as there should be debonding between the fiber and the matrix because of the great difference in their stiffness modulus. Complete breakage of the sample does not happen because of the limitations of the finite element code, in which the stiffness matrix becomes singular as soon as a particle, or node, detaches from the rest of the body and is not constrained any longer. There are ways to control this behavior up to a certain point: reduce the applied strain at each step, so that fracture happens slowly and particles tend to stay attached to the main body longer (this method was used in the present work); make the code a dynamic code, with time as a variable, which should prevent the stiffness matrix to become singular; change the behavior of the truss elements from completely brittle to plastic, or add an unloading curve so that the bonds do not break too suddenly; never actually delete elements, but bring their stiffness very close to zero once damage happens.

The second case analyzed is a hexagonal RVE with a volume fraction $V_f = 15\%$ and an interface elements

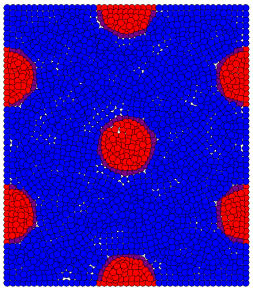

(a) $\epsilon = 0\%$

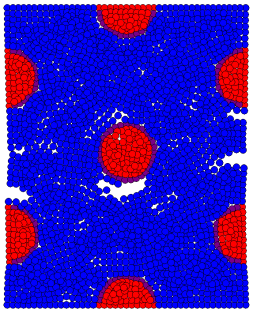

(b) $\epsilon = 4\%$

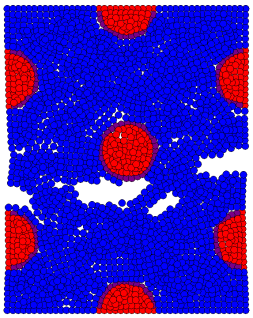

(c) $\epsilon = 4.8\%$

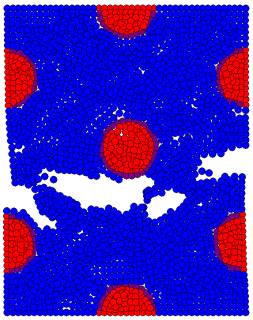

(d) $\epsilon = 5.3\%$

Figure 3.16: Hexagonal RVE, $V_f = 10\%$, $E_{int} = 500$ GPa

stiffnes of 500 GPa and it is shown in Figure 3.17. The ultimate toughness of the interface elements is kept at 100 GPa. The plate is in tension, with and applied $\epsilon = 0.001$ at the top and bottom sides until a final strain of 4.2% is reached. In this case as well debonding happens between three fibers and the matrix, as can be seen in Figure 3.17b. As the plate is being pulled further the fractures propagate until they eventually join each other and shown in Figure 3.17d. Contrarily to what happened in the previous case ($V_f = 10\%$), there is no damage initiation except for debonding, because the high volume fracture does not leave enough room for the matrix to initiate crack in the middle of the sample. The behavior shown is expected and agrees with experience for this type of problem and the result is obtained without providing additional information to the analysis, such as crack nucleation criterion or a softening model.

The last case studied in the present thesis is a hexagonal RVE with a volume fraction $V_f = 10\%$ and an interface elements stiffnes of 5000 GPa. The stiff interface is used to try to simulate a plate with perfect bonding between the fiber and the matrix. The ultimate toughness of the interface elements is kept at 100 GPa. The plate is in tension, with and applied $\epsilon = 0.0005$ at the top and bottom sides until a final strain of 8.25% is reached. The result is shown in Figure 3.18. In 3.18b crack initiates at the center of the plates on the two sides, while debonding starts happening at the middle fiber. Contrarily to what happens in Figure 3.16b there is no debonding between the matrix and the fibers on the sides, due to the high stiffness of the interface elements. The fractures in the plate propagate naturally until they eventually join each other at $\epsilon = 8.25\%$ and the plate is completely broken. The goal of this analysis was to check whether peridynamics could predict the behavior of a fiber composite plate undergoing fracture; it was shown that peridynamics seems to be able to naturally model the behavior of a plate in tension undergoing fracture, in this case until complete breakage. Although a lot more testing and research is needed for the analysis of this type of material, the present work shows that peridynamics is a promising method with the potential to become a complete toold for stress and fracture analysis in composite materials.

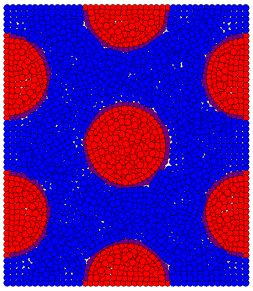

(a) $\epsilon = 0\%$

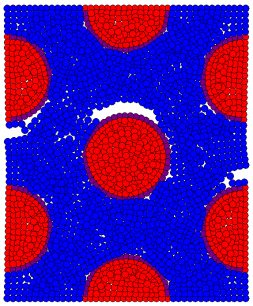

(b) $\epsilon = 2.8\%$

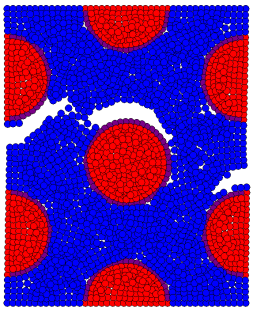

(c) $\epsilon = 3.5\%$

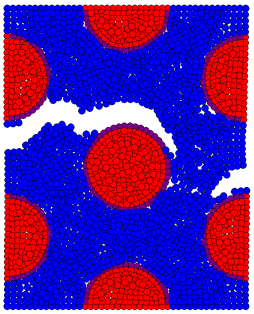

(d) $\epsilon = 4.2\%$

Figure 3.17: Hexagonal RVE, $V_f = 15\%$, $E_{int} = 500$ GPa

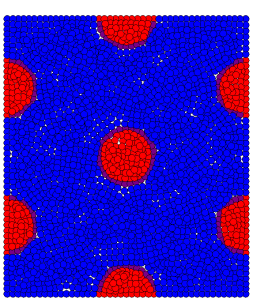

(a) $\epsilon = 0\%$

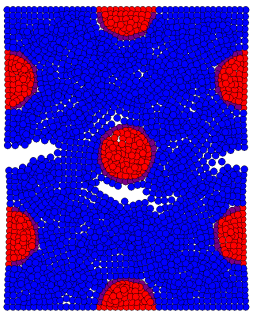

(b) $\epsilon = 4\%$

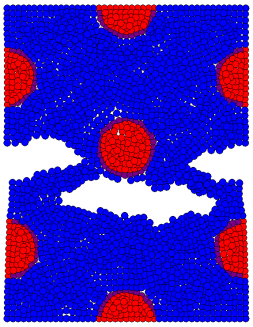

(c) $\epsilon = 6.5\%$

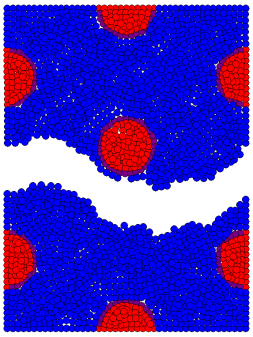

(d) $\epsilon = 8.25\%$

Figure 3.18: Hexagonal RVE, $V_f = 10\%$, $E_{int} = 5000$ GPa

Chapter 4

Conclusions

A nonlocal continuum theory called peridynamics is analyzed and implemented in a finite element framework. The pairwise force function that acts along the line between particles in the original peridynamics theory is substituted by one-dimensional truss elements, the mechanical properties of which are related to the macroscale properties of the material being analyzed through energy relations. The nonlocality of the model is given by a quantity called horizon, which sets a limit for the interaction of particle laying within a finite distance δ. The fact that peridynamics can be implemented in a finite element frame allows to simplify the coding process and the verification of the code itself because of the known analytical solutions to truss problems; furthermore, it is discussed how the finite element implementation reduces computational time compared to other meshless codes.

It is shown that peridynamics can approximate the stress distribution in a 2-D hollow aluminum plate in tension both qualitatively and quantitatively with good accuracy. The displacement in the vertical direction is also in good agreement with the analytical solution, while the displacement in the horizontal direction appears not to be very accurate. The reasons for such inaccuracies can be sought in the sparse mesh (especially near the hollow part in the center of the sample) and in the lack of a normalization factor in the

truss elements close to the boundaries. Fracture on a hollow plate in tension is analyzed using peridynamics to study how cracks form and propagate in the sample. It is shown that fracture naturally happens as a consequences of the strain in the truss members as well as the fall of particles outside other particles' horizon. There is no need for extra information about the location of the crack and the propagation of damage does not seem to be mesh dependent, although this is hard to see when using a small regular mesh as the one employed in this work. The crack seems to be forming in the right location and propagate horizontally until complete breakage of the sample is reached, which is expected from experience.

A composite plate with an inclusion, too, is studied using peridynamics implemented in a finite element framework. The matrix of the plate is made of the polymer EPON 862, while the circular inclusion is made of a dual-layer carbon nanotube (CNT). The plate is in tension and the results are compared to the analytical solution for an infinite plate with no interface, meaning that there is perfect bonding between the two phases of the composite plate. The stiffness modulus for interface truss elements is taken as an average of the elastic modulus of the matrix and inclusion elements. The displacements obtained are in not very good agreement with the analytical solution, especially as we get closer to the inclusion at the center of the plate. The stress distribution obtained computationally seems to suffer from instability (oscillations are present in the solution) and poor mesh refinement, which leads to a solution that is not accurate and does not compare well to the analytical solution. Apart from the sparse mesh (especially near the inclusion), the causes for the poor accuracy of the model can be sought in the lack of a normalization factor near the boundaries, the arbitrary choice of the stiffness of the interface elements, as well as inherent properties of the peridynamics model when this type of composite problem is approached: the horizon might vary from material to material, the nonlocality between two different phases might be defined in a different way and some more information about the interface might be needed to obtain a better and a more credible solution. Fracture on the composite plate is also analyzed by gradually putting the plate in tension on the top and bottom sides. As expected, debonding between the two phases happens, dictated by the greatly different material properties and yield stretch of the truss elements of the two materials. Damage happens naturally in

the right locations and extends horizontally until it reaches the sides of the plate, causing complete breakage of the sample. This is confirmed by a finite element code employing the cohesive zone methodvand proves that peridynamics is a natural and consistent method for predicting and modeling fracture analysis in solids.

The last case studied is a hexagonal RVE with different volume fractions and different stiffness of the interface elements. This qualitative study showed that peridynamics can predict debonding and fracture propagation with good accuracy, with no need for additional parameters. It is shown that fracture happens naturally and that the different damage modes join each other until complete breakage of the samples is achieved. Again, peridynamics seems to be a promising tool for the analysis of this type of problems and can be employed to predict damage propagation in solids.

Chapter 5

Future Challenges

The implementation of peridynamics in a finite element framework, although less computationally expensive than its meshless counterpart, requires a fine mesh to catch all the material behaviors under different types of loading, especially during fracture. The fine mesh, since every node is connected to many other nodes that lie inside its horizon, requires high computational power or better efficiency of the code. In the future the code written for this work should be translated to a better performing language such as FORTRAN or C, should be run on more powerful machines and could employ parallel computing to exploit all of its potential. Instead of regular rectangular meshes, a random arrangement of the particles (nodes) should be employed, which is a better representation of the randomness in the physical world.

Another improvement to the code will be making it able to handle three-dimensional problems, to be able to analyze a greater range of cases and address many challenges of fracture dynamics, including impact problems and high-rate fracture problems. By making the code able to handle dynamic problems with time as a variable one will be able to account for stress waves and their effect on the propagation of damage in solids, as well as finding and modeling crack propagation velocity and branching.

As stated in the goals of the present work, the fact that this code is built from scratch allows for great

personalization. This means that composite materials can be analyzed throughly and their implementation in peridynamics can be studied to make it as consistent as possible. This requires theoretical work as well as computational validation and can be obtained through a deeper analysis of the peridynamic model for this particular class of problems. The same thing can be said for piezoresistive materials, which can eventually be modeled using peridynamic theory by adding electrical properties to the single bonds or truss elements. The development of the peridynamic theory and its application to the most diverse fields look exciting and very promising.

Bibliography

[1] Gates, T., Odegard, G., Frankland, S., and Clancy, T., "Computational materials: Multi-scale modeling and simulation of nanostructured materials," *Composites Science and Technology*, Vol. 65, 2005, pp. 2416–2434, [used with permission of Elsevier].

[2] Lehoucq, R., "Peridynamics for multiscale materials modeling," Sandia National Labs, 2008, Power Point Presentation, [used with permission of R. Lehoucq].

[3] Silling, S. and Askari, E., "A meshfree method based on the peridynamic model of solid mechanics," *Computers and Structures*, Vol. 83, 2005, pp. 1526–1535, [used with permission of Elsevier].

[4] Hu, W., Ha, Y., and Bobaru, F., "Peridynamic model for dynamic fracture in unidirectional fiber-reinforced composites," *Comput. Methods Appl. Mech. Engrg.*, Vol. 217-220, 2012, pp. 247–261, [used with permission of Elsevier].

[5] Seleson, P., Parks, M., Gunzburger, M., and Lehoucq, B., "Peridynamic as an upscaling of molecular dynamics," *Multiscale Modeling Simulations*, Vol. 8, No. 1, 2009, pp. 204–227, [copyright ©2009 Society for Industrial and Applied Mathematics. Reprinted with permission. All rights reserved].

[6] Uang, C., Gilbert, A., Zamecnik, S., and Rokach, S., *Fundamentals of structural analysis*, chap. 4, McGraw-Hill, 2011.

[7] De Pablo, J. and Curtin, W., "MRS Bulletin," *Cambridge University Press*, Vol. 32, No. 11, 2007, pp. 905–911.

[8] Hashin, Z., "Analysis of composite materials - A survey," *Journal of Applied Mechanics*, Vol. 50, 1983, pp. 481–505.

[9] Seidel, G. and Lagoudas, C., "Micromechanical analysis of the effective elastic properties of carbon nanotube reinforced composites," *Mechanics of Materials*, Vol. 38, 2006, pp. 884–907.

[10] Silling, S., "Reformulation of elasticity theory for discontinuities and long-range forces," *Journal of the Mechanics and Physics of Solids*, Vol. 48, 2000, pp. 175–209.

[11] Macek, R. and Silling, S., "Peridynamics via finite element analysis," *Finite Elements in Analysis and Design*, Vol. 43, 2007, pp. 1169–1178.

[12] Bazant, Z. and Jirasek, M., "Nonlocal Integral Formulations of Plasticity and Damage: Survey of Progress," *American Society of Civil Engineers*, Vol. 128, 2002, pp. 1119–1149.

[13] Eringen, A., "A unified theory of thermomechanical materials," *International Journal of Engineering Science*, Vol. 4, 1966, pp. 179–202.

[14] Cosserat, E. and Cosserat, F., "Thorie des Corps dformables," *Scientific Library A. Hermann and Sons*, Vol. 1, 1909, pp. 1–226.

[15] Neff, P. and Jeong, J., "The linear isotropic Cosserat (micropolar) model," .

[16] Mindlin, R., "Micro-structure in linear elasticity," *Archive for Rational Mechanics and Analysis*, Vol. 16, 1964, pp. 51–78.

[17] Kunin, I., "The theory of elastic media with microstructure and the theory of dislocations," *Mechanics of generalized continua*, 1968, pp. 321–329.

[18] Krumhansl, J. and Kroner, E., "Mechanics of generalized continua," *Springer Verlag, Berlin*, 1968, pp. 298.

[19] Edelen, D., "Protoelastic bodies with large deformations," *Archive for Rational Mechanics and Analysis*, Vol. 34, 1969, pp. 283–300.

[20] Eringen, C., *Nonlinear theory of continuous media*, McGraw-Hill, 1962.

[21] Eringen, C., "Simple microfluids," *International Journal of Engineering Science*, Vol. 2, 1964, pp. 205–217.

[22] Eringen, C. and Suhubi, E., "Nonlinear theory of simple micro-elastic solids," *International Journal of Engineering Science*, Vol. 2, 1964, pp. 189–203.

[23] Eringen, A., "Theory of micropolar continua," *Proceedings of the Ninth Midwestern Mechanics Conference*, 1965, p. 23.

[24] Eringen, C., "Theory of thermo-microstretch elastic solids," *International Journal of Engineering Science*, Vol. 28, 1990, pp. 1291–1301.

[25] Eringen, C., "Theory of thermo-microstretch fluids and bubbly liquids," *International Journal of Engineering Science*, Vol. 28, 1990, pp. 133–143.

[26] Eringen, C., *Mechanics of micromorphic continua*, Defense Technical Information Center, 1967.

[27] Kafadar, C. and Eringen, C., "Micropolar media - I, the classical theory," *International Journal of Engineering Science*, Vol. 9, 1971, pp. 271–305.

[28] Eringen, C., "Nonlocal polar elastic continua," *International Journal of Engineering Science*, Vol. 10, 1972, pp. 1–16.

[29] Eringen, C., "On nonlocal microfluid mechanics," *International Journal of Engineering Science*, Vol. 11, 1973, pp. 291–306.

[30] Aero, E. and Kuvshinskii, E., "Fundamental equations of the theory of elastic media with rotationally interacting particles," *Fiz. Tverd. Tela*, Vol. 2, No. 7, 1960, pp. 1399–1409.

[31] Grioli, G., "Elasticit asimmetrica," *Annali di Matematica Pura e Applicata*, Vol. 50, 1960, pp. 389–417.

[32] Rajagopal, E., "The existence of interfacial couples in infinitesimal elasticity," *Annalen der Physik*, Vol. 461, No. 3-4, 1960, pp. 192–201.

[33] Toupin, R., "Elastic materials with couple-stresses," *Archive for Rational Mechanics and Analysis*, Vol. 11, 1962, pp. 385–414.

[34] Mindlin, R., "Second gradient of strain and surface-tension in linear elasticity," *International Journal of Solids and Structures*, Vol. 1, No. 4, 1965, pp. 417–438.

[35] Green, A. and Rivlin, R., "Simple force and stress multipoles," *Archive for Rational Mechanics and Analysis*, Vol. 16, No. 5, 1964, pp. 325–353.

[36] Kruhmansl, J., *Some considerations on the relations between solid state physics and deneralized continuum mechanics*, Defense Technical Information Center, 1968, pp. 298–331.

[37] Jirasek, M., "Nonlocal models for damage and fracture: comparison of approaches," *International Journal of Solid Structures*, Vol. 35, 1997, pp. 4133–4145.

[38] Eringen, A. and Edelen, D., "On nonlocal elasticity," *International Journal of Engineering Science*, Vol. 10, 1972, pp. 233–248.

[39] Rogula, D., "Influence of spatial acoustic dispersion od dynamicalproperties of dislocations," *Bull. Acad. Pol. Sci., Ser. Sci. Tech.*, Vol. 13, 1965, pp. 337–343.

[40] Kroner, E., "Continuum mechanics and range of atomic cohesion forces," *Proc., 1st Int. Conf. on Fracture*, edited by T. K. T. Yokobori and e. J. Swedlow, Japanese Society for Strength and Fracture of Materials, Sendai, Japan, 1966.

[41] Kroner, E., "Elasticity theory of materials with long range cohesive forces," *Int. J. Solids Struct.*, Vol. 3, 1967, pp. 731–742.

[42] Kroner, E. and Datta, B., "Nichtlokale Elastostatik: Ableitung aus der Gittertheorie," *Z. Phys.*, Vol. 196, 1966, pp. 203–211.

[43] Kunin, I., "Model of elastic medium simple structure with spatial dispersion," *Prikl. Mat. Mekh.*, Vol. 30, 1966, pp. 942.

[44] Kunin, I., "Theory of elasticity with spatial dispersion," *Prikl. Mat. Mekh.*, Vol. 30, 1966, pp. 866.

[45] Edelen, D. and Laws, N., "On the thermodynamics of systems with nonlocality," *Arch. Ration. Mech. Anal.*, Vol. 43, 1971, pp. 24–35.

[46] Pijaudier-Cabot, G. and Bazant, Z., "Nonlocal damage theory," *J. Eng. Mech.*, Vol. 113, No. 10, 1987, pp. 1512–1533.

[47] Bazant, Z. and Pijaudier-Cabot, G., "Nonlocal continuum damage, localization instability and convergence," *Journal of Applied Mechanics*, Vol. 55, 1988, pp. 287–290.

[48] Bazant, Z. and Chang, T., "Nonlocal finite Element analysis of strain softening solids," *J. Eng. Mech.*, Vol. 113, No. 1, 1987, pp. 89–105.

[49] Polizzotto, C., "Nonlocal elasticity and related variational principles," *International Journal of Solids and Structures*, Vol. 38, No. 42-43, 2001, pp. 7359–7380.

[50] Polizzotto, C., "Unified thermodynamic framework for nonlocal/gradient continuum theories," *European Journal of Mechanics - A/Solids*, Vol. 22, No. 5, 2003, pp. 651–668.

[51] Rogula, D., "Introduction to nonlocal theory of material media," *Nonlocal theory of material media, CISM courses and lectures*, Vol. 268, 1982, pp. 125–222.

[52] Barenblatt, G., *Scaling, self-similarity, and intermediate asymptotics*, Vol. 14, cambridge university press ed., 1996.

[53] Bazant, Z. and Pijaudier-Cabot, G., "Measurement of characteristic length of nonlocal continuum," *Journal of Engineering Mechanics*, Vol. 115, 1989, pp. 755–767.

[54] Bobaru, F. and Hu, W., "The meaning, selection and use of the peridynamic horizon and its relation to crack branching in brittle materials," *Letters in Fracture and Micromechanics*, Vol. 176, 2012, pp. 215–222.

[55] Ramulu, M., Kobayashi, A., Kang, B., and Barker, D., "Further studies on dynamic crack branching," *Experimental Mechanics*, Vol. 23, No. 4, 1983, pp. 431–437.

[56] Ramulu, M. and Kobayashi, A., "Mechanics of crack curving and branching: a dynamic fracture analysis," *International Journal of Fracture*, Vol. 27, 1985, pp. 187–201.

[57] Streit, R. and Finnie, L., "An experimental investigation of crack-path directional stability," *Experimental Mechanics*, Vol. 20, No. 1, 1980, pp. 17–23.

[58] Lehoucq, R. and Silling, S., "Convergence of Peridynamics to Classical Elasticity Theory," *Journal of Elasticity*, Vol. 93, 2008, pp. 13–37.

[59] Bobaru, F., Mijia, Y., Alves, L., Silling, S., Askari, E., and Xu, J., "Convergence, adaptive refinement, and scaling in 1D peridynamics," *International Journal for Numerical Methods in Engineering*, Vol. 77, 2009, pp. 852–877.

[60] Silling, S., Epton, M., Weckner, O., Xu, J., and Askari, E., "Peridynamic states and constitutive modeling," *Journal of Elasticity*, , No. 88, 2007, pp. 151–184.

[61] Parks, M., Lehoucq, R., Plimpton, S., and Silling, S., "Implementing peridynamics within a molecular dynamics code," *Computer Physics Communications*, Vol. 179, 2008, pp. 777–783.

[62] Teran, J., Sifakis, E., Irving, G., and Fedkiw, R., "Robust quasistatic finite elements and flesh simulations," *Eurographics/ACM SIGGRAPH Symposium on Computer Animation*, 2005.

[63] Bobaru, F. and Ha, Y., "Adaptive refinement and multiscale modeling in 2D peridynamics," *International Journal for Multiscale Computational Engineering*, Vol. 9, No. 6, 2011, pp. 635–660, [copyright ©2011, with permission from Begell House, Inc. Reprinted with permission. All rights reserved].

[64] Kasayapanand, N., "Exact solution of a double filled hole of an infinite plate," *Mechanics of Materials and Structures*, Vol. 3, 2008, pp. 365–373.